A QUANTUM MECHANICAL SEMICONDUCTOR DEVICE SIMULATOR

by

Imran Ahmed Bhutta

Dissertation submitted to the Faculty of the
Virginia Polytechnic Institute and State University
in partial fulfillment of the requirements for the degree of
DOCTOR OF PHILOSOPHY
in
Electrical Engineering

APPROVED:

Aicha Elshabini-Riad
Chairperson

Sedki M. Riad
Co-Chairperson

Ioannis M. Besieris

Samir El-Ghazaly

Daniel J. Moore

July, 1994
Blacksburg, Virginia

A Quantum Mechanical Semiconductor Device Simulator

by

Imran A. Bhutta

Co-Chairpersons: Aicha Elshabini-Riad, and Sedki M. Riad

Abstract

Semiconductor device simulators have generally been based on either classical or semi-classical approaches. In these approaches, the Poisson's equation is solved with either the current continuity equation or the Boltzmann transport equation. Methods based on quantum mechanics have been generally very computer intensive, and thus until recently not much favored. However, with the availability of faster and more powerful computers this picture is changing. As the physical dimensions of the semiconductor devices are reduced, the assumptions made in the classical and the semi-classical approaches become invalid and the simulation results become inaccurate. For such cases, quantum mechanical concepts must be introduced to provide accurate simulation results.

This dissertation presents the proof of concept of a semiconductor device simulator based on the quantum mechanical principals. The simulation technique is based on the self consistent solution of the Poisson's and time independent Schrödinger wave equation for a 1-D finite differenced grid. The applicability of the technique to a 2-D finite differenced grid is also presented. The simulation is performed by first solving for the Fermi energy distribution inside the simulation domain. The initial estimates about the carrier concentrations are developed from the Fermi energy distribution. Based on the carrier concentrations, the potential distribution inside the device is updated using the Poisson's equation. The updated potential distribution is then used in the time independent Schrödinger's equation and the carrier wave vectors are thus determined. The carrier wave vectors, along with appropriate density of state function and distribution function are used to update the carrier concentrations. For the 1-D case, the density of state function is based on a single dimension of a three dimensional volume with the assumption that the density of states is the same for all the three dimensions. The distribution function used is the Fermi-Dirac distribution function. The new carrier concentrations thus computed are then substituted back into the Poisson's equation, and self consistency is obtained when minimum error criteria has been met.

The device simulator has the capability of simulating heterojunctions semiconductor devices fabricated from elemental semiconductors such as Si and Ge, as well as binary and tertiary compound semiconductors.

Acknowledgments

All of us at one time or another have received help from another human being. I have been fortunate to always have caring people around me who have helped and guided me. I am indebted to so many that it would be impossible to thank every one. Nevertheless I would like to take this opportunity to acknowledge a few.

Foremost, I would like to thank God for providing me with opportunities to avail. Without His love and support I could not have accomplished anything.

I would like to thank my family for their endless love, support and faith in my abilities. In particular, I would like to thank my parents, Mr. Waqar Ahmed Bhutta and Mrs. Hamidah Waqar. They taught me the values which I hold so dear. My everlasting love and thanks go to my wife Saima for her support and understanding. She took more than her share of work so that I could concentrate on my research. I would also like to thank my brother Bilal and his family for providing me with an environment of love and support. I cherish my friendship with my brother, his helpful suggestions were key factors in solving some of the technical problems.

I would also like to thank my advisors Dr. Aicha Elshabini-Riad and Dr. Sedki M. Riad. I could not have had better advisors than them. Their trust in me has been a key factor in developing my abilities. They have treated me as a family member and helped me every step of the way. I owe them my everlasting gratitude. I would also like to thank my committee members, Dr. Daniel J. Moore, Dr. Ioannis M. Besieris, and especially Dr. Samir El-Ghazaly. Their expertise and suggestions have been essential in the successful completion of this research.

Finally, I would like to thank all my colleagues with whom I have worked all these years. I am proud to be part of such a fine group. I value their friendship and am grateful to them for providing me with an excellent environment to work in.

Table of Contents

List of Figures and Tables

Chapter 1

Introduction

With the development of the first semiconductor diode (Germanium diode) by Karl Lark-Horovitz and his group at Purdue University in 1942, and the development of the first transistor by John Bardeen, Walter Brattain and William Shockley at Bell Telephone Research Laboratories in 1947, the electronic community was heralded into a new era. Soon, new devices ('pnp' transistor in 1951, planar transistor in 1958, MOSFET in 1962) and new concepts (Integrated Circuit in 1959, Microprocessor in 1971) were developed which established the reliability and efficiency of semiconductor devices. The rate of development of semiconductor devices has been phenomenal, with minimum feature size shrinking at the rate of 11% per year and semiconductor chip area increasing by about 19% per year [1.1]. These developments have brought the electronic community a long way from those early days. At the present time, devices span from multiple quantum wells to submicron geometry microprocessors. This high rate of device development has only been made possible by better understanding of the operation and behavior of these electronics devices and their materials. The original semiconductor devices were developed with the help of a better understanding of the underlying quantum physics of the semiconductor materials.

1.1 Early development of quantum mechanics

Quantum mechanics had its beginning in the 17th century with the observation by Isaac Newton that light may be regarded as consisting of particles. However, particle nature of light could not be proved until the end of the 19th century with the discovery of the photoelectric effect by Albert Einstein. In 1924, De Broglie suggested the duality of particle and wave nature of all matter [1.2]. De Broglie hypothesis was based on the Heisenberg's uncertainty principle and Planck's constant.

$$(\Delta x)(\Delta p) \approx h \tag{1.1}$$

where,

Δx = uncertainty in position (x).

Δp = uncertainty in momentum (p).

h = Planck's constant, ($6.6260755 \times 10^{-34}$ J-s)

De Broglie gave the wavelength associated with the wave like nature of every matter as,

$$\lambda = \frac{h}{p} \tag{1.2}$$

De Broglie hypothesis claimed that every matter particle has an associated frequency and exhibits wave like properties. The wavelike nature is more visible in particles with small

momentum, and the reason one does not observe the wave like nature of matter of large masses or large energy is due to the smallness of Planck's constant.

In order to explain the De Broglie waves, Erwin Schrödinger at the insistence of Debye in 1926 developed the wave equation, currently referred to as Schrödinger wave equation. The equation was developed by starting from the conservation of energy principle.

$$E_{Total} = E_{Kinetic} + E_{Potential} \tag{1.3}$$

where,

E_{Total} = Total energy of the object.

$E_{Kinetic}$ = Kinetic energy of the object.

$E_{Potential}$ = Potential energy of the object.

From Newtonian mechanics,

$$E_{Kinetic} = \frac{p^2}{2m} \tag{1.4}$$

where,

m = Mass of the object.

Now from equation (1.2),

$$p = \frac{h}{\lambda} \tag{1.5}$$

Substituting equation (1.5) in equation (1.4),

$$E_{Kinetic} = \frac{h^2}{2m\lambda^2} = \frac{(h/2\pi)^2}{2m(\lambda/2\pi)^2} \tag{1.6}$$

$$E_{Kinetic} = \frac{\hbar^2}{2m}k^2 \tag{1.7}$$

where,

$\hbar$ = Reduced Planck's constant ($h / 2\pi$).

k = Propagation number ($2\pi / \lambda$).

In terms of mathematical operators, 'k' can be expressed as,

$$k = -i\frac{\partial}{\partial x} \tag{1.8}$$

Thus equation (1.3) becomes,

$$E_{Total} = -\frac{h^2}{2m}\frac{\partial^2}{\partial x^2} + V \tag{1.9}$$

where,

V = Potential energy.

Consider that there is a function, $\psi(x,t)$, which has two basic properties;

1) The function can interfere with itself. This property can be used to predict diffraction effects.
2) The function must be large where the particle is most likely to be and small every place else. The square of this function thus provides the probability of finding the particle.

If equation (1.9) is made to operate on a function satisfying the above conditions, then that function can describe the behavior of a single particle of mass m, possessing energy equal to E_{Total}, and under the influence of an external force V. Equation (1.9) thus takes on the one dimensional time dependent form of Schrödinger's wave equation.

$$E\psi(x,t) = -\frac{\hbar^2}{2m}\frac{\partial^2\psi(x,t)}{\partial x^2} + V\psi(x,t) \qquad (1.10)$$

Many of the semiconductor materials are crystalline in nature. The periodicity of the fixed atoms in the crystal introduces forces that effect the transport of the charged carriers. To compensate for these forces due to the crystalline nature of the semiconductor material, the mass of the charged carrier is changed. The new masses are called density of state effective masses, and depend upon the band gap variation of the crystal in the different directions. Therefore the mass, m, in equation (1.10) is replaced by the density of state effective mass term m^*.

Therefore, Schrödinger's wave equation at any point r, can be written as,

$$E\psi(r,t) = -\frac{\hbar^2}{2m^*}\nabla^2\psi(r,t) + V\psi(r,t) \tag{1.11}$$

which in its time independent form becomes,

$$E\psi(r) = -\frac{\hbar^2}{2m^*}\nabla^2\psi(r) + V\psi(r) \tag{1.12}$$

Earlier in 1913, Niels Bohr had expounded on the Johan Jakob Balmer's spectral formula and developed a model for electrons orbiting the nucleus of an atom. Bohr's model gave quantized energy levels for the electrons. Electrons could only possess these energy levels and not any energy in between. Due to the orbital motion of the electron around the nucleus, the electron also possess an angular momentum. In 1925, George Uhlenbeck and Sam Goudsmit suggested that beside having an angular momentum, the electrons also possessed a spin about their axis. This spin was the result of the quantization of the angular momentum. The same year Wolfgang Pauli proposed the exclusion principle, known as "Pauli's exclusion principle". The principle states that the no two electrons can have the same spin and the same quantized energy levels. In fact, Pauli's exclusion principle applies to all fermions with the exception of bosons such as photons.

Not all of the important discoveries related to electronic devices and semiconductors were due to the development of quantum mechanics. One of the most fundamental equations relating to electricity and magnetism are the Maxwell's equations. In 1885, James Clerk Maxwell introduced his equations for electromagnetism. Maxwell's equations in their differential form are;

$$\nabla \times \mathscr{E} = -\mathscr{M}_i - \frac{\partial \mathscr{B}}{\partial t} \tag{1.13}$$

$$\nabla \times \mathscr{H} = \mathscr{J}_i + \mathscr{J}_c + \frac{\partial \mathscr{D}}{\partial t} \tag{1.14}$$

$$\nabla \bullet \mathscr{D} = q_{ev} \tag{1.15}$$

$$\nabla \bullet \mathscr{B} = q_{mv} \tag{1.16}$$

where,

$\mathscr{E}$ = Electric field intensity.

$\mathscr{H}$ = Magnetic field intensity.

$\mathscr{D}$ = Electric flux density.

$\mathscr{B}$ = Magnetic flux density.

$\mathscr{J}_i$ = Impressed electric current density.

$\mathscr{J}_c$ = Conduction electric current density.

$\mathscr{M}_i$ = Impressed magnetic current density.

q_{ev} = Electric charge density.

q_{mv} = Magnetic charge density.

The constitutive relations are,

$$\mathscr{D} = \varepsilon \mathscr{E} \tag{1.17}$$

$$\mathscr{B} = \mu \mathscr{H} \tag{1.18}$$

$$\mathscr{J}_c = \sigma \mathscr{E} \tag{1.19}$$

where,

ε = Permittivity of the medium.

μ = Permeability of the medium.

σ = Conductivity of the medium.

In general, permittivity is a tensor, however for semiconductor materials of diamond or zinc-blende crystalline structures, permittivity becomes scalar. Furthermore, eventhough Maxwell's equations hold true in any media, the constitutive relations are only valid at relatively small electric and magnetic fields and not very high frequencies. Therefore, under these conditions, equations (1.15) and (1.17) can be combined, thus giving the familiar form of Poisson's equation.

$$\nabla \bullet (\varepsilon \mathscr{E}) = \rho_{ch} \tag{1.20}$$

Fundamental discoveries in quantum mechanics continue untill the present time. However, these early quantum mechanical discoveries may be sufficient to provide some understanding for the operation of semiconductor devices and their materials.

In this work, Poisson's equation and Schrödinger's wave equation are the two fundamental equations which will be solved under the appropriate boundary conditions to simulate the operation of the semiconductor device.

1.2 Early development of semiconductor device models and simulators

Equivalent circuit modeling techniques were available when the first semiconductor devices were produced. Therefore, a natural extension was made and the equivalent circuit models of the new devices were developed. These models are based on the electrical characteristics of the device, and find wide use in circuit simulations.

In 1949, Shockley developed the p-n junction theory along the lines of an analytical model with many simplifying assumptions. Ebers-Moll's 1954 theory of Bipolar junction transistor was based along the same lines. These models treated the devices as one dimensional, with constant impurity profiles in the different regions. The neutral and space charge regions were treated differently, and appropriate boundary conditions were taken to link the two regions. These models have been quite successful in describing the

device behavior. However, the simplifying assumptions are no longer valid in the quantum regime of current devices. The increased complexity of current devices has rendered the analytical models as unpractical, and new approaches to studying device behavior and performance are required. Semiconductor device simulation is one such approach used to study the semiconductor device behavior under certain specified working conditions.

One of the first attempts at numerical simulation of semiconductor devices was taken by H. K. Gummel in 1964 when he introduced a one dimensional model of Silicon BJT. By 1966, statistical techniques such as Monte Carlo had been introduced by T. Kurosawa for the solution of carrier transport, and by 1969 D. L. Scharfetter and H. K. Gummel introduced their current continuity algorithm, for one dimensional simulation of Silicon Read diode. With the advent of planar devices, carrier transport became a two dimensional process, thus requiring two dimensional simulation approach. One of the first two dimensional simulation of a Silicon BJT was introduced by D. P. Kennedy and R. R. O'Brien in 1970.

Complex structures of some of the present day devices, in particular small geometry FETs, have forced the use of three dimensional device simulators. Starting in early 1980s, three dimensional device simulators started appearing, however these device simulators require significant computer resources, and thus have not been very actively used.

In the past fifteen years, the electronics industry has seen a tremendous surge in the development of new semiconductor materials, and novel devices. Designer have been able to bring devices to the market in a timely fashion, using modeling and simulation techniques capable of predicting the device behavior in a variety of circuit configurations and environmental conditions. Looking back, it is safe to say that semiconductor device simulators represent an important part of the design and development process.

This dissertation work deals with the development of a semiconductor device simulator using the quantum mechanical approach. The device simulator is proposed to be a general purpose simulator capable of predicting device performance for a variety of materials and geometries. The device simulator is developed starting from a one dimensional approach and the methodology is then extended to two dimensions. The layout of the dissertation has been kept systematic. Chapter I is a brief introduction to the different concepts used in the work. Chapter II presents the literature survey of previous work in similar fields. Chapter III describes the need for this particular approach towards device modeling. Chapter IV and V present the solution method and simulation results, respectively. Conclusion and future directiuons are presented in chapter VI. A list of references is presented at the end.

Chapter 2

Summary of Previous Literature

2.1 Overview of Equivalent Circuit Models

As mentioned in the introduction, electrical equivalent circuit modeling techniques predate semiconductor devices and thus were naturally adopted to the emerging devices. Electrical equivalent circuit models are primarily used in circuit analysis. An electronic circuit usually contains active devices, in addition to passive components. While the current and voltage behavior of passive devices is defined by simple relationships, the equivalent relationships in active devices are quite complicated in nature [2.1]. Therefore, in order to analyze an active circuit, the devices are replaced by equivalent circuit models that give the same output characteristics as the active device itself. These models are made up of passive elements, voltage sources, and current sources. Equivalent circuit models provide the designer with reasonably accurate values for frequencies below 1 GHz for Bipolar Junction Transistors (BJTs), and their use is very popular in circuit analysis software [2.2]. Some Field Effect Transistor (FET) models are accurate up to 10 GHz. However, as the analysis frequency increases, so does the model complexity. Since the Equivalent Circuit Models are based on some fundamental equations describing the device behavior, they can also be used to predict the characteristics of the device itself.

When performing circuit analysis, two important factors which must be taken into account are the speed and accuracy of computation. Sometimes, the computation speed can be considerably improved by simplifying the equivalent circuit model, without significant loss in computation accuracy. For this reason, there are a number of equivalent circuit models depending upon the device application and related conditions. Equivalent circuit models have been developed for Diodes, Bipolar Junction Transistors (BJTs), as well as Field Effect Transistors (FETs). In this overview, the equivalent circuit models for BJT and FET devices are presented.

Most of the equivalent circuits for BJTs are based on the Ebers-Moll model [2.3] or the Gummel-Poon model [2.4]. The original Ebers-Moll model was a large signal, nonlinear DC model for BJTs. Since then, a number of improvements have been incorporated to make the model more accurate for various applications. In addition, an accurate model has been introduced by Gummel and Poon.

There are three main types of equivalent circuit models, depending upon the device signal strength. On this basis, the models can be classified as follows:

1) Large Signal Equivalent Circuit Model
2) Small Signal Equivalent Circuit Model.
3) DC Equivalent Circuit Model.

Use of the large signal or small signal model depends upon the magnitude of the driving source. In applications where the driving currents or the driving voltages have large amplitudes, large signal models are used. In circuits where the signal does not deviate much from the DC biasing point, small signal models are more suitable. For DC conditions and very low frequency applications, DC equivalent circuit models are used. For DC and very low frequency analysis, the circuit element values can be assumed to be lumped, whereas in high frequency analysis, incremental element values give much more precise results.

2.1.1 Large Signal Equivalent Circuit Model

Depending upon the frequency of operation, large signal equivalent circuit models can be further classified as:

1) High Frequency Large Signal Equivalent Circuit Model
2) Low Frequency Large Signal Equivalent Circuit Model

For each of the two above cases, a BJT and a FET model will be presented.

2.1.1.1 High Frequency Large Signal Equivalent Circuit Model of a BJT

In this context, high frequency denotes frequencies above 10 kHz. In the equivalent circuit model, the transistor is assumed to be composed of two back-to-back diodes. Two current-dependent current sources are added to model the current flowing through the reverse biased base-collector junction and the forward biased base-emitter junction. Two junction capacitances, C_{jE} and C_{jC}, model the fixed charges in the emitter-base space charge region and base-collector space charge region, respectively. Two diffusion capacitances, C_{DE} and C_{DC}, model the corresponding charge associated with mobile carriers, while the base resistance, r_b, represents the voltage drop in the base region. All the above circuit elements are very strong functions of operating frequency, signal strength, and bias voltage.

The high frequency large signal equivalent circuit model of an npn BJT is shown in Figure 2.1, where the capacitances C_{jE}, C_{jC}, C_{DE}, C_{DC} are defined as follows:

$$C_{jE}\left(V_{B'E'}\right) = \frac{C_{jEO}}{\left(1 - \frac{V_{B'E'}}{\phi_E}\right)^{m_E}} \tag{2.1}$$

where,

$V_{B'E'}$ = Internal base-emitter voltage.

C_{jEO} = Base-emitter junction capacitance at $V_{B'E'} = 0$.

ϕ_E = Base-emitter barrier potential.

m_E = Base-emitter capacitance gradient factor.

$$C_{jC}\left(V_{B'C'}\right) = \frac{C_{jCO}}{\left(1 - \frac{V_{B'C'}}{\phi_C}\right)^{m_C}} \tag{2.2}$$

where,

$V_{B'C'}$ = Internal base-collector voltage.

C_{jCO} = Base-collector junction capacitance at $V_{B'C'} = 0$.

ϕ_C = Base-collector barrier potential.

m_C = Base-collector capacitance gradient factor.

$$C_{DE} = \frac{\tau_F I_{CC}}{V_{B'E'}} \tag{2.3}$$

where,

I_{CC} = Collector reference current.

τ_F = Total forward transit time.

$$C_{DC} = \frac{\tau_R I_{EC}}{V_{B'E'}} \tag{2.4}$$

where,

I_{EC} = Emitter reference current.

τ_R = Total reverse transit time.

α_R and α_F are the large signal reverse and forward current gains of a common base transistor, respectively.

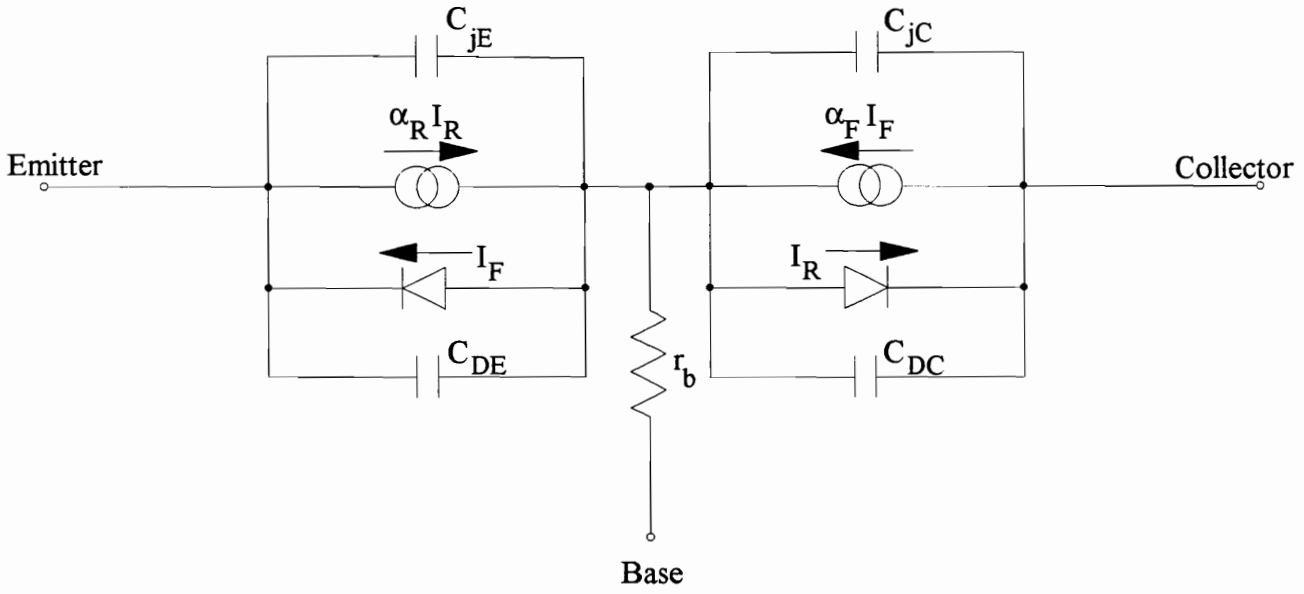

Figure 2.1, High Frequency Large Signal Model of a BJT

This circuit can be made linear by replacing the forward biased base-emitter diode with a low value resistor, r_π, while the reverse biased base-collector diode is replaced with a high value resistor, r_μ. The junction and diffusion capacitors are lumped together to form C_π and C_μ, while the two current sources are lumped into one source given by,

$$(g_{mF}V_F - g_{mR}V_R) \tag{2.5}$$

where,

g_{mF} = Forward transconductance.

g_{mR} = Reverse transconductance.

V_F = Voltage across the forward biased diode.

V_R = Voltage across the reverse biased diode.

The two diodes are represented by r_π and r_μ. r_π is typically about 3 KΩ, while r_μ is more than a few MΩ, and C_π is about 120 pF. The linear circuit representation is illustrated in Figure 2.2.

The Gummel-Poon representation is very similar to the high frequency large signal linear circuit model of Figure 2.2. However, the terms describing the elements are different and a little more involved.

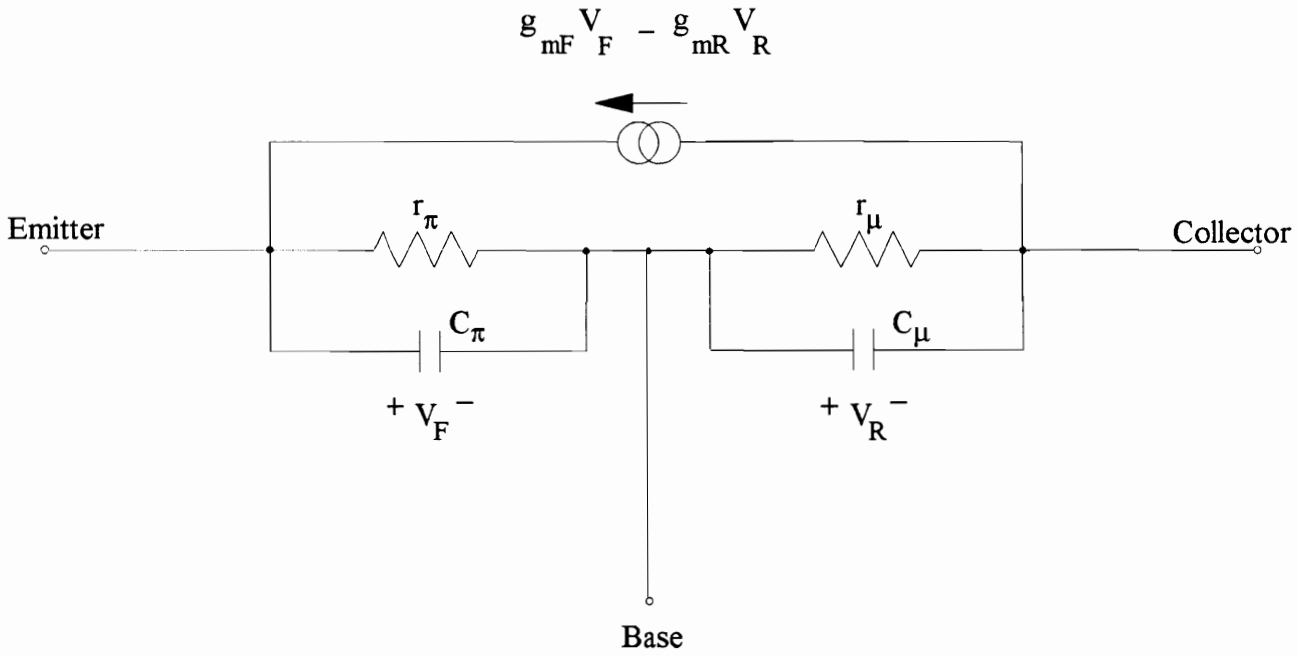

Figure 2.2, Linear Circuit Representation of High Frequency Large Signal Model of a BJT

2.1.1.2 High Frequency Large Signal Equivalent Circuit Model of a FET

In the high frequency large signal equivalent circuit model of a FET, the fixed charge stored between the gate and the source and between the gate and the drain are modeled by the gate-to-source and the gate-to-drain capacitances, C_{GS} and C_{GD}, respectively. The mobile charges between the drain and the source are modeled by the drain-to-source capacitance, C_{DS}. The voltage drop through the active channel is modeled by the drain-to-source resistance, R_{DS}. The current through the channel is modeled by a voltage-controlled current source. For large signals, the gate is sometimes driven into the forward region, and thus the conductance through the gate is modeled by the gate conductance, G_g. The conductance from the gate to the drain and from the gate to the source is modeled by the gate-to-drain and gate-to-source resistances, R_{GD} and R_{GS}, respectively. A variable resistor, R_i, is added to model the gate charging time such that the time constant:

$$R_i C_{GS} = \text{Constant} \tag{2.6}$$

For MOSFETs, typical element values are: C_{GS} and C_{GD} are in the range of 1 - 10 pF, C_{DS} is in the range of 0.1 - 1 pF, R_{DS} is in the range of 1 - 50 KΩ, R_{GD} is more than $10^{14}\Omega$, R_{GS} is more than $10^{10}\Omega$, and g_m is in the range of 0.1 - 20 mA/V. Figure 2.3 illustrates the high frequency large signal equivalent model of a FET.

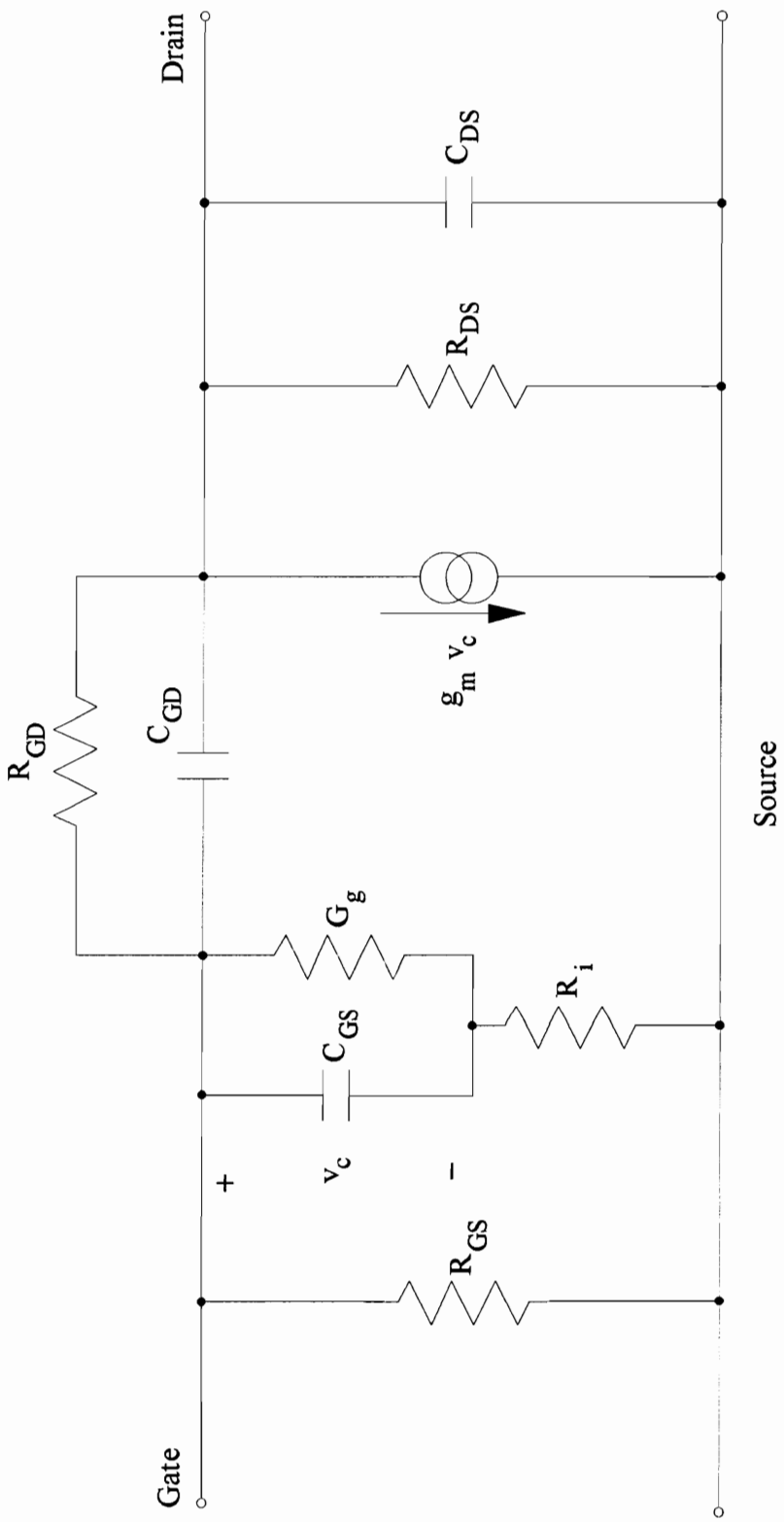

Figure 2.3, High Frequency Large Signal Model of a FET

2.1.1.3 Low Frequency Large Signal Equivalent Circuit Model of a BJT

In this case, low frequency denotes frequencies below 10 kHz. The low frequency large signal equivalent circuit model of a BJT is based on its DC characteristics. Whereas at high frequencies, one has to take incremental values to obtain accurate analysis, at low frequencies the average of these incremental values yields same level of accuracy in the analysis. Therefore, in low frequency analysis, the circuit elements of the high frequency model are replaced by their average values. The low frequency large signal equivalent circuit model is shown in Figure 2.4.

2.1.1.4 Low Frequency Large Signal Equivalent Circuit Model of a FET

Because of their very high reactance values the gate-to-source, gate-to-drain and drain-to-source capacitances can be assumed as open circuits, at low frequencies. Therefore the low frequency large signal model is similar to the high frequency large signal model, except that it has no capacitances. The resulting circuit describing low frequency operation is shown in Figure 2.5.

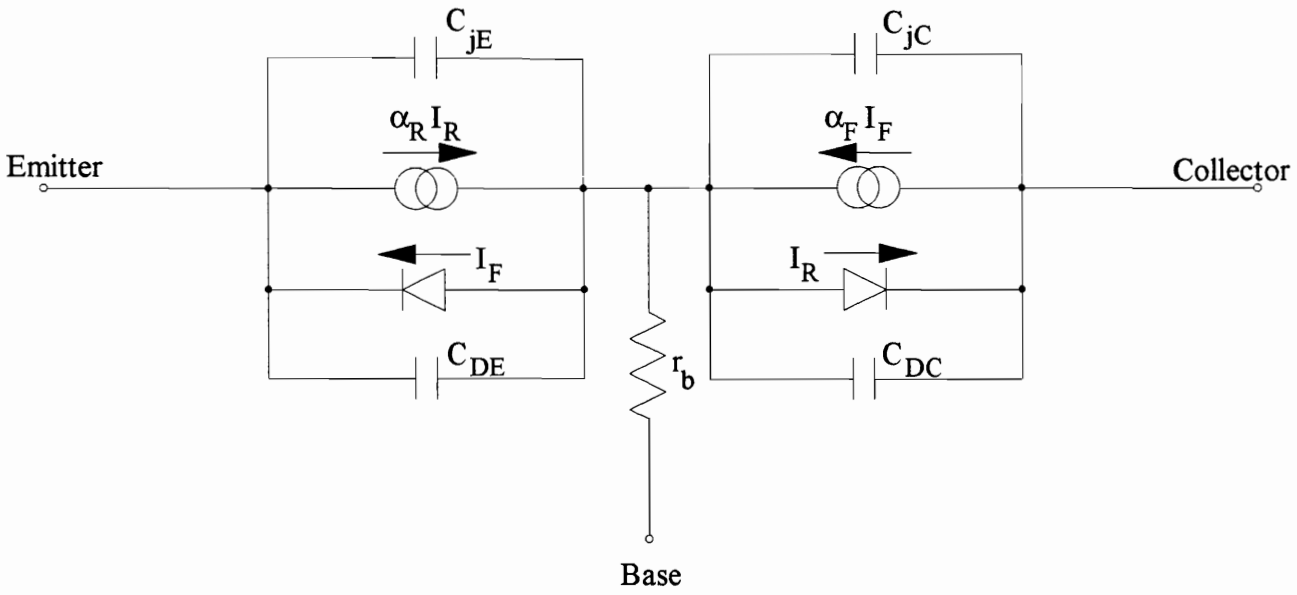

Figure 2.4, Low Frequency Large Signal Model of a BJT

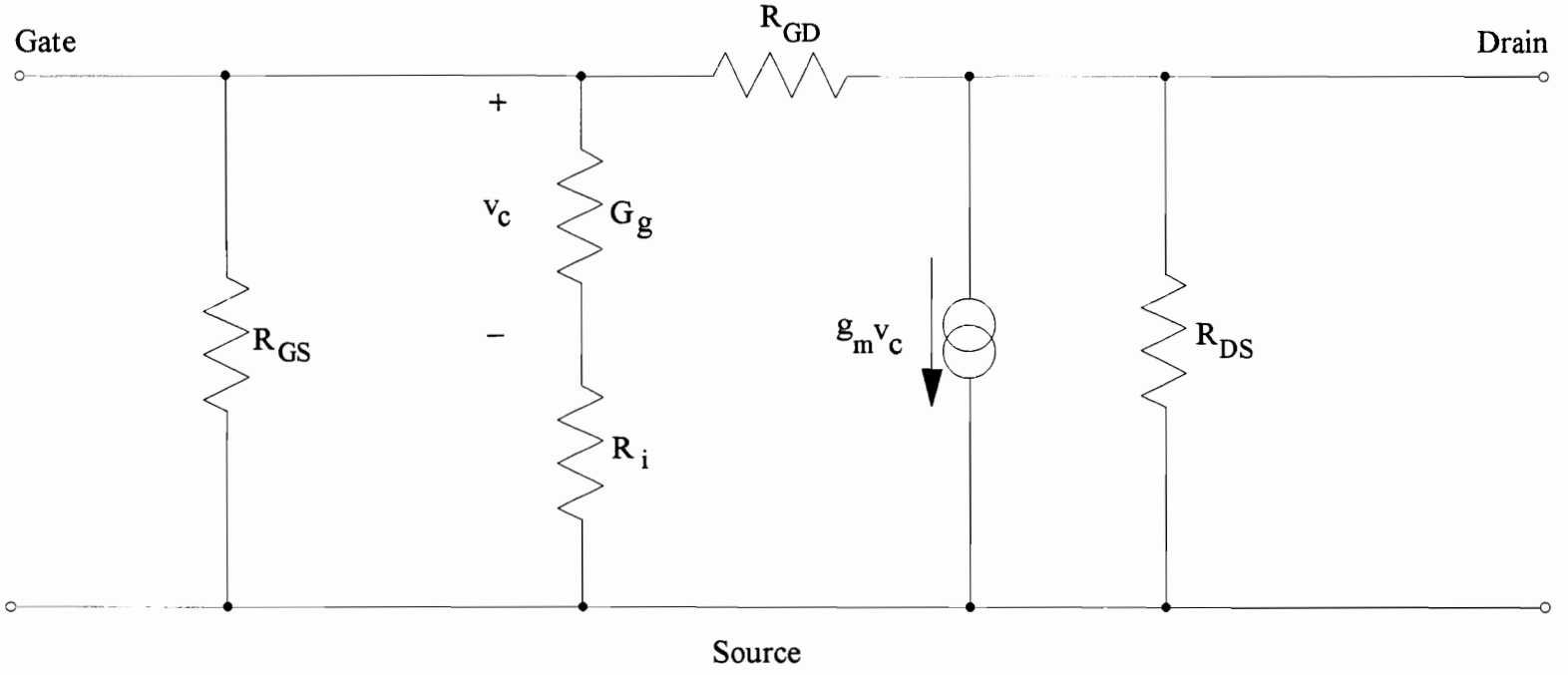

Figure 2.5, Low Frequency Large Signal Model of a FET

2.1.2 Small Signal Equivalent Circuit Model

In a small signal equivalent circuit model, the signal variations around the DC-bias operating point are very small. As for the large signal model, there are two types of small signal models, depending upon the operating frequency:

1) High Frequency Small Signal Equivalent Circuit Model
2) Low Frequency Small Signal Equivalent Circuit Model

Again a BJT and a FET model for each of the above two cases will be presented.

2.1.2.1 High Frequency Small Signal Equivalent Circuit Model of a BJT

The high frequency small signal equivalent circuit model of a BJT is very similar to its high frequency large signal equivalent circuit model. However in the small signal model, in addition to the base resistance r_b, the emitter and collector resistances, r_e and r_c, respectively are added to the circuit. The emitter resistance is usually very small due to high emitter doping used to obtain better emitter injection efficiency. Therefore, whereas at large signal strengths the effect of r_e is overshadowed by the base resistance, at small signal strengths this emitter resistance cannot be neglected. The collector resistance

becomes important in the linear region, where the collector-emitter voltage is low. The high frequency small signal equivalent circuit model is shown in Figure 2.6.

2.1.2.2 High Frequency Small Signal Equivalent Circuit Model of a FET

For small signal operations, the signal strength is not large enough to forward bias the gate-to-semiconductor diode; hence no current will flow from the gate to either the drain or the source. Therefore the gate-to-source and gate-to-drain series resistances, R_{GS} and R_{GD}, can be neglected. Also, since there will be no current flow from the gate to the channel, the gate conductance, G_g, can be also be neglected. Figure 2.7, illustrates the high frequency small signal equivalent circuit model of a FET.

2.1.2.3 Low Frequency Small Signal Equivalent Circuit Model of a BJT

As in the low frequency large signal model, the junction capacitances, C_{jC} and C_{jE}, and the diffusion capacitances, C_{DE} and C_{DC}, can be neglected. Furthermore, the base resistance, r_b, can also be neglected. Since the voltage drop across the base is not significant and the variations in the base width caused by changes in the collector-base voltage are also very small. The low frequency small signal equivalent circuit model is shown in Figure 2.8.

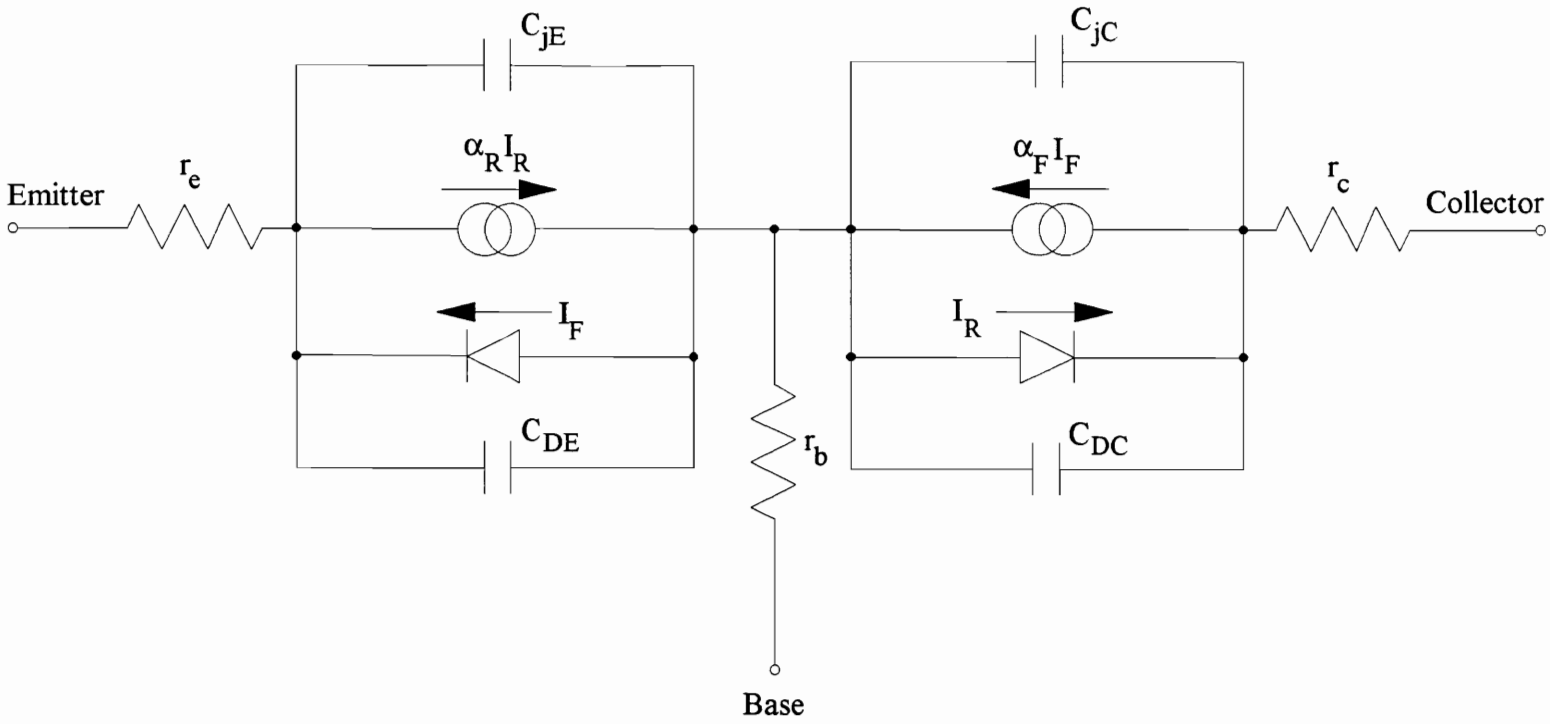

Figure 2.6, High Frequency Small Signal Model of a BJT

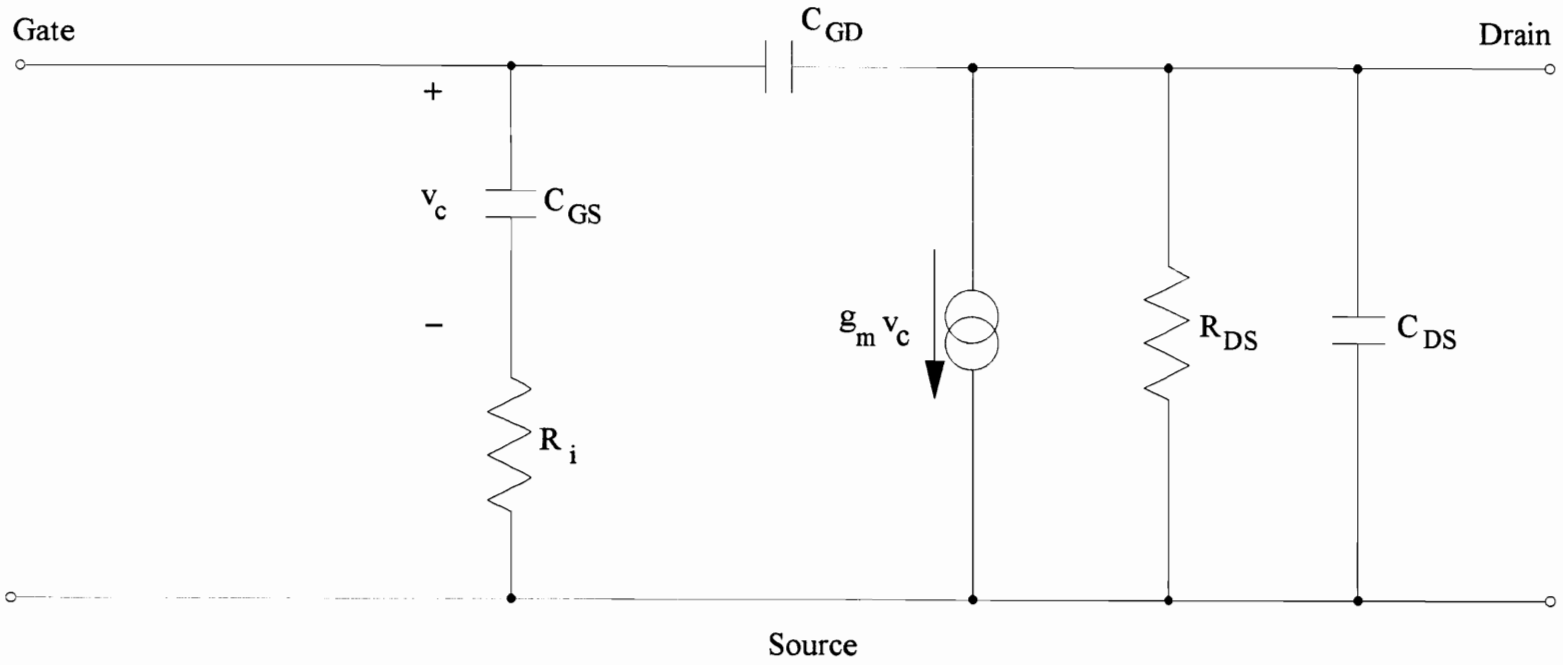

Figure 2.7, High Frequency Small Signal Model of a FET

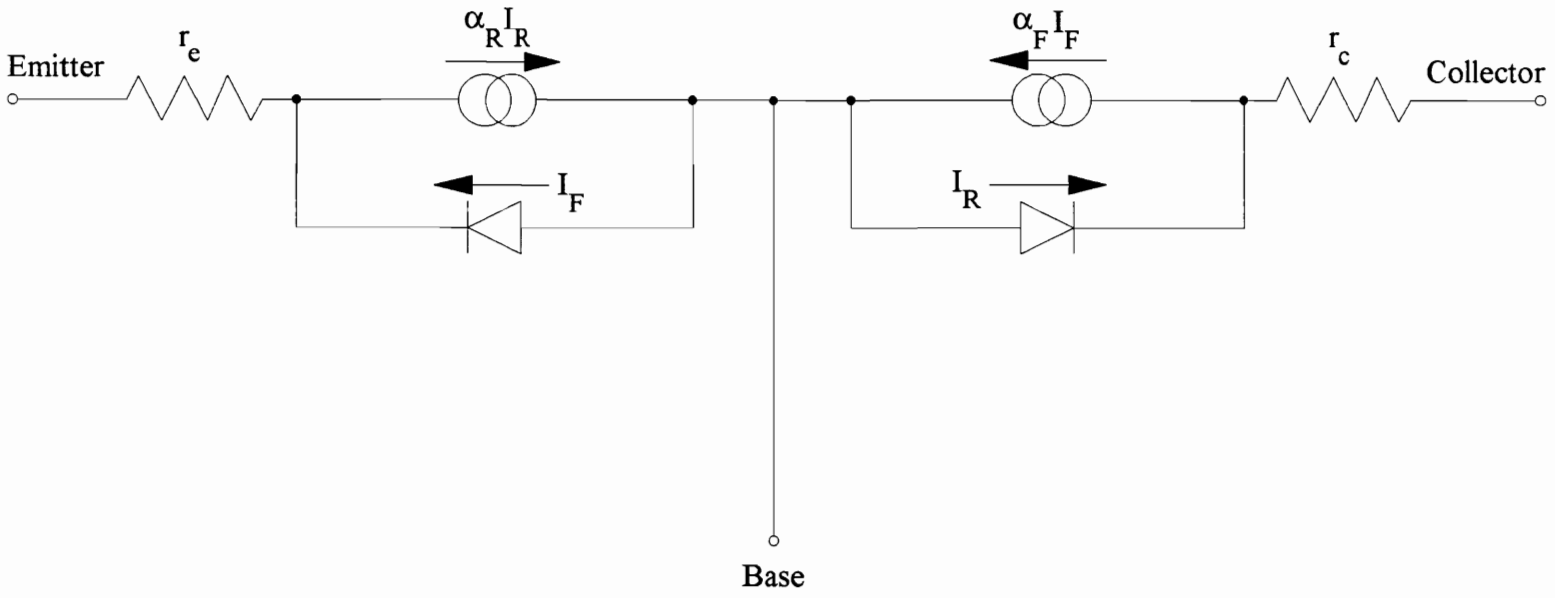

Figure 2.8, Low Frequency Small Signal Model of a BJT

2.1.2.4 Low Frequency Small Signal Equivalent Circuit Model of a FET

Since the reactances associated with all the capacitances are very high, one can neglect the capacitances for low frequency analysis. The gate conductance as well as the gate-to-source and gate-to-drain resistances can also be neglected, because this is a small signal operation. The resulting low frequency equivalent circuit model of a FET is shown in Figure 2.9.

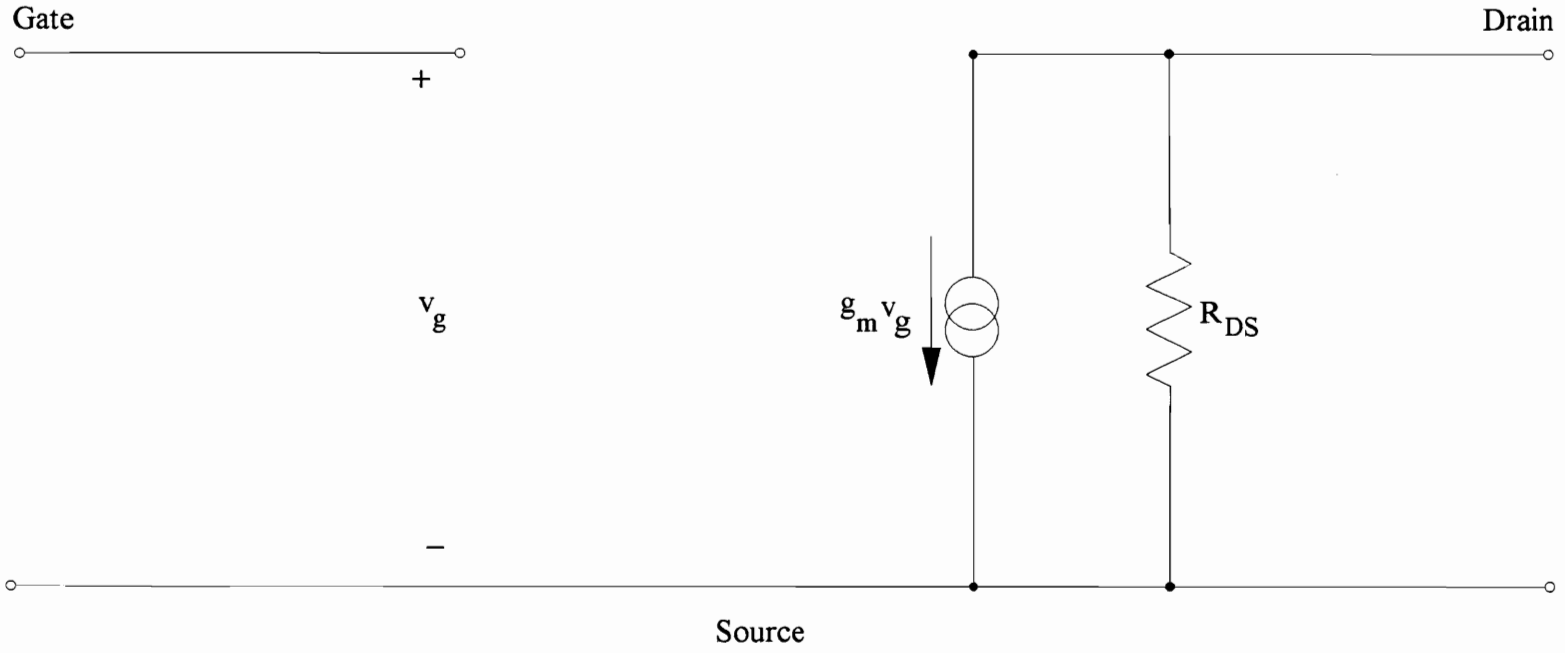

Figure 2.9, Low Frequency Small Signal Model of a FET

2.1.3 DC Equivalent Circuit Model

DC equivalent circuit models for a BJT and a FET are presented.

2.1.3.1 DC Equivalent Circuit Model of a BJT

The DC equivalent circuit model of a BJT is based on the original Ebers-Moll model. Such models are employed when the transistor is used at DC or in applications where the operating frequency is below 1 kHz.

There are two versions of the DC equivalent circuit model; the *injection version* and the *transport version*. The difference between the two versions lies in the choice of the reference current. In the *injection version*, the reference currents are I_F and I_R, the forward and reversed biased diode currents, respectively. In the *transport version*, the reference currents are I_{CC} and I_{CE} , the collector and emitter transport currents, respectively. These currents are of the form:

$$I_F = I_{ES}\left[\exp\left(\frac{qV_{BE}}{kT}\right) - 1\right] \tag{2.7}$$

where,

I_{ES} = Base-emitter saturation current.

V_{BE} = Base-emitter voltage.

$$I_R = I_{CS}\left[\exp\left(\frac{qV_{BC}}{kT}\right) - 1\right] \tag{2.8}$$

where,

I_{CS} = Base-collector saturation current.

V_{BC} = Base-collector voltage.

$$I_{CC} = I_S\left[\exp\left(\frac{qV_{BE}}{kT}\right) - 1\right] \tag{2.9}$$

where,

I_S = Saturation current.

$$I_{EC} = I_S\left[\exp\left(\frac{qV_{BC}}{kT}\right) - 1\right] \tag{2.10}$$

In most computer simulations, the *transport version* is usually preferred because of the following conditions:

1) I_{CC} and I_{EC} are ideal over many decades.

2) I_S can specify both reference currents at any given voltage.

The DC equivalent circuit model of a BJT is shown in Figure 2.10.

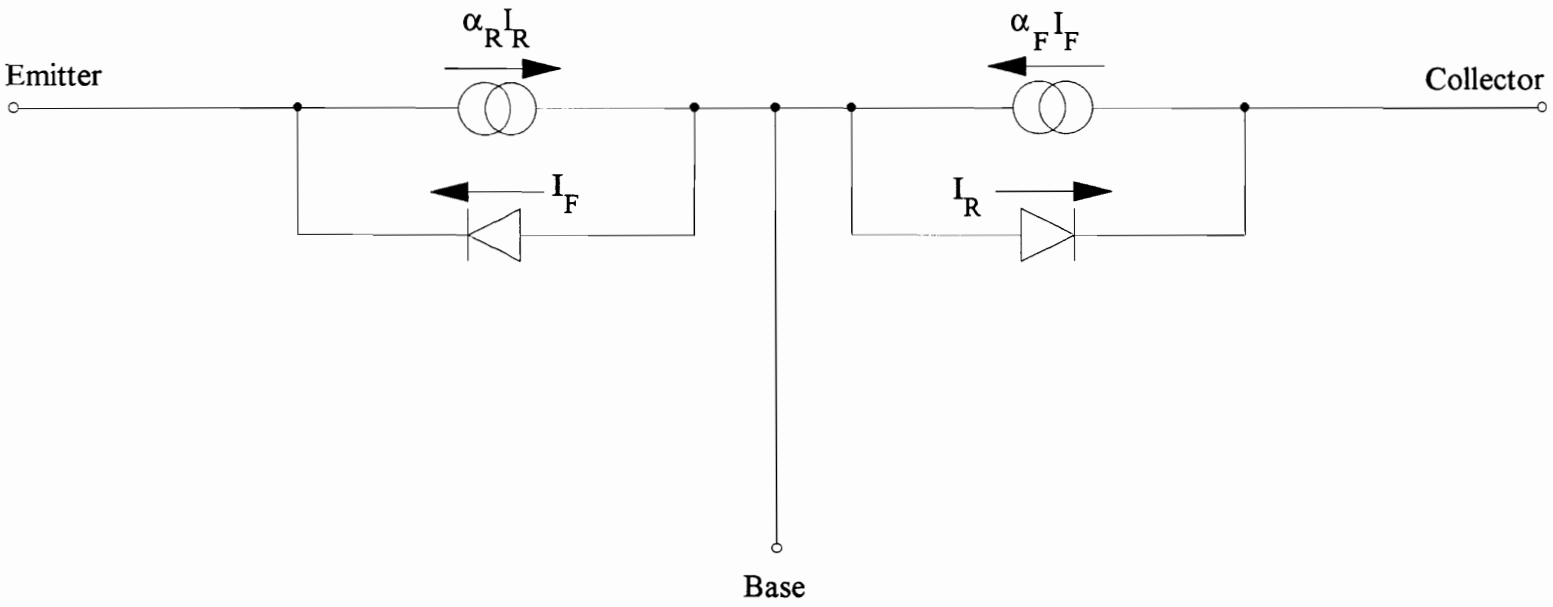

Figure 2.10, DC Equivalent Circuit Model of a BJT

2.1.3.2 *DC Equivalent Circuit Model of a FET*

In the DC equivalent circuit model of a FET, the gate is considered isolated because the gate-semiconductor interface is formed as a reverse-biased diode and therefore is open circuited. All capacitances are also assumed to represent open circuits. R_{GS}, R_{GD}, R_i and R_{DS} are neglected since there is no conductance through the gate and, because this is a DC analysis, there are no charging effects associated with the gate. The DC equivalent circuit of a FET is illustrated in Figure 2.11.

2.1.4 *Commercially Available Software Packages*

A number of circuit analysis software packages commercially available, one of the most widely used being SPICE [2.5]. In this package, the BJT models are a combination of the Gummel-Poon and modified Ebers-Moll models. Figure 2.12 shows a common emitter transistor circuit, and a SPICE input file, containing the transistor model. Some other available packages are SLIC [2.6], SINC [2.7] and SITCAP [2.8].

Equivalent circuit models are basically used to replace the semiconductor device in an electronic circuit. These models are developed from an understanding of the device's current and voltage behavior. However, equivalent circuit models cannot predict 3-D effects or device behavior for novel devices where internal device operation is not well

understood. For such situations the designer has another tool available, the Semiconductor Device Simulator.

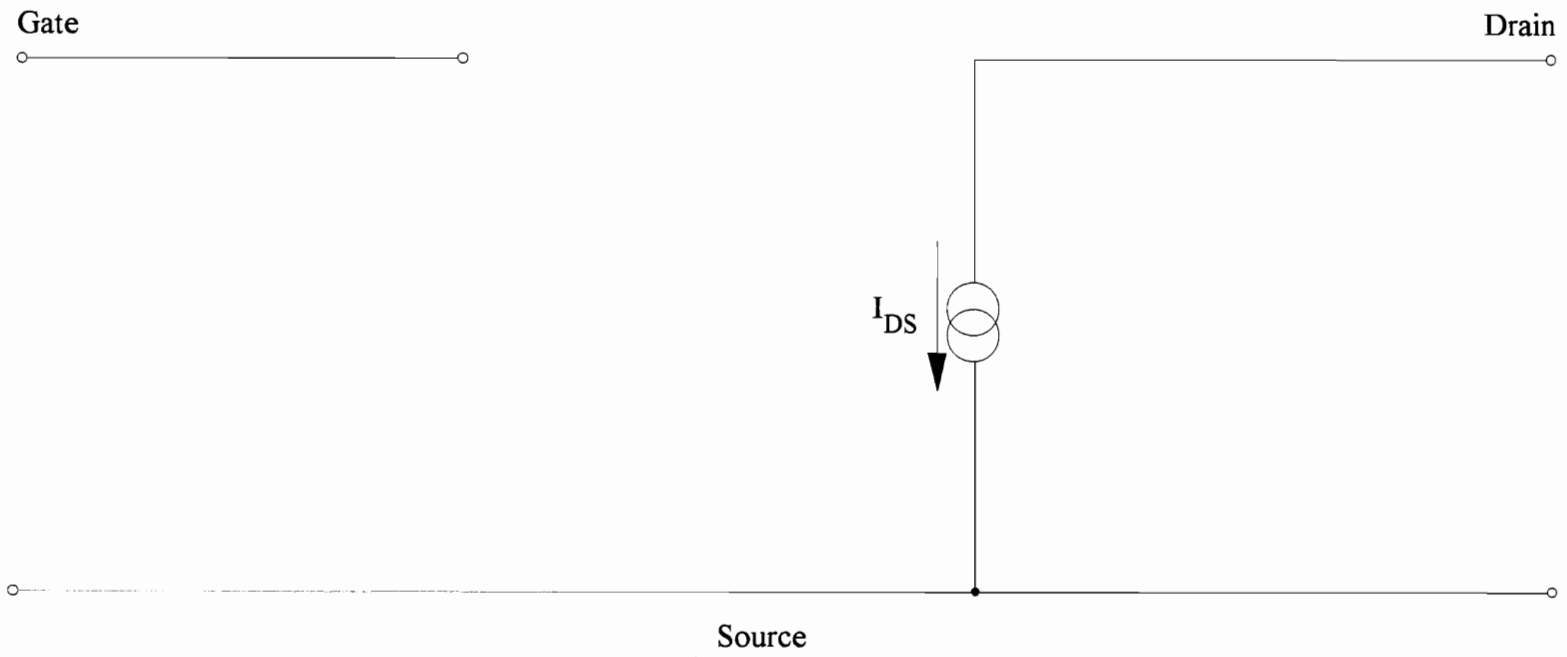

Figure 2.11, DC Equivalent Circuit Model of a FET

```
VS 1 0 DC 0.0 AC 75e-3 sin(0 75m 10k); sin(offset, peak amp, freq, delay, damping, phase)
VCC 4 0 12.0
*
*Resistor elements
*
Rs 1 2 1 Kohm
R1 4 3 225K
R2 3 0 47K
RC 4 5 5.1K
RE 6 0 1K
RL 7 0 2K
*
*Capacitor elements
*
C1 2 3 3.3UFd
C2 51 7 3.3UF
C3 6 0 47UF
*
*Voltage Sources for Current measurements
*
VB 3 31 0.0
VC 5 51 0.0
VE 61 6 0.0
*
*Transistor (Collector-Base-Emitter)
*
Q1 51 31 61 MQNOM
.model MQNOM NPN (BF = 130 CJE = 25pF CJC = 8pF)
*
.AC dec 25 10 10MEG; Freq Variation from 10 Hz- 10 MHz
.tran 1u 200u 100u; Step size, duration, start point
.Probe
.End
```

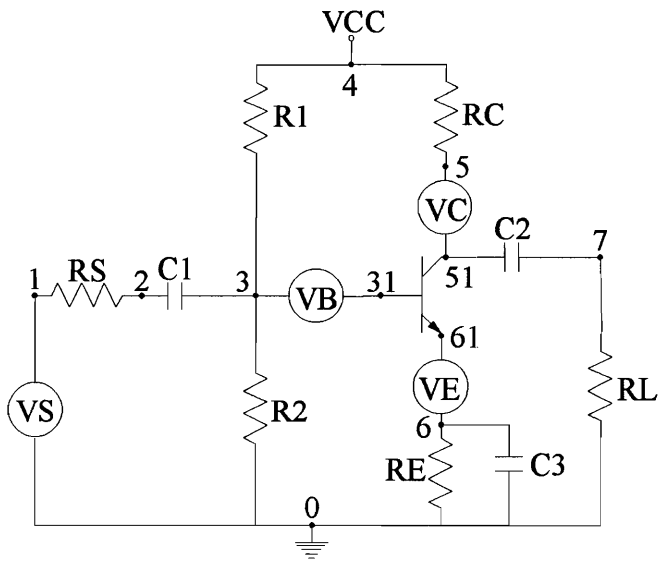

Transistor model

Figure 2.12, Typical Common Emitter BJT Circuit and its' SPICE File

2.2 Overview of Semiconductor Device Simulators

Device simulators are based on the physics of semiconductor devices [2.9, 2.10]. The input to the simulator takes the form of information about the device under consideration such as material type, device dimensions, doping concentrations and operating conditions. Based on this information, the device simulator computes the electric field inside the device and thus predicts carrier concentrations in the different regions of the device. Device simulators can also predict transient behavior, including quantities such as current-voltage characteristics, and frequency bandwidth. There are three basic approaches to device simulation:

1) Classical approach.
2) Semi-classical approach.
3) Quantum mechanical approach.

2.2.1 Device Simulators Based on Classical Approach

The classical approach is based on the solution of Poisson's equation and the current continuity equations. The current is comprised of the drift and the diffusion current components.

2.2.1.1 Assumptions

The equations for the classical approach can be obtained by making the following approximations to the Boltzmann Transport Equation:

i) Carrier temperature is the same throughout the device and is assumed to equal the lattice temperature.

ii) Quasi steady-state conditions exist.

iii) Carrier mean free path must be smaller than the distance over which the quasi Fermi level is changing by kT/q.

iv) The impurity concentration is constant or varies very slowly along the mean free path of the carrier.

v) Energy band is parabolic.

vi) Influence of the boundary conditions is negligible.

For general purposes, even with these assumptions and limitations, the models based on the classical approach give fairly accurate results. The model assumes that the driving force for the carriers is the quasi Fermi potential gradient, which is also dependent upon the electric field value. Therefore, in some simulators, the quasi Fermi level distributions are computed and the carrier distribution is estimated from this information.

2.2.1.2 Equations to be Solved

With the assumption of a quasi steady-state condition, the operating wavelength is much larger than the device dimensions. Hence, from equation (1.20) we can write the Poisson's equation for non-homogeneous medium as,

$$\nabla \bullet (\varepsilon \nabla V) = -q_{ev} \tag{2.11}$$

with,

$$-\nabla V = E \tag{2.12}$$

where,

V = Potential of the region under simulation.

ε = Permittivity of the medium under simulation.

q_{ev} = Charge enclosed by the simulation region.

E = Electric field inside the simulation region.

Also from Maxwell's equations, we can determine the current continuity equations for a homogeneous medium as:

$$\nabla \bullet J_n - q\left(\frac{\partial n}{\partial t}\right) = +qU \tag{2.13}$$

with,

$$J_n = q\mu_n nE + qD_n \nabla \bullet n \tag{2.14}$$

where,

J_n = Electron current density.

n = Electron concentration.

D_n = Electron diffusion coefficient.

μ_n = Electron mobility.

U = Generation-Recombination term.

q = Electronic charge ($1.6021917 \times 10^{-19}$ C).

and

$$\nabla \bullet J_p + q\left(\frac{\partial p}{\partial t}\right) = -qU \tag{2.15}$$

with,

$$J_p = q\mu_p pE - qD_p \nabla \bullet p \tag{2.16}$$

where,

J_p = Hole current density.

p = Hole concentration.

D_p = Hole diffusion coefficient.

μ_p = Hole mobility.

For non-homogeneous media, the electric field term in the current expressions is modified to account for the non-uniform density-of-states and the band gap variation [2.11].

In the classical approach, the objective is to calculate the potential and the carrier distribution inside the device. Poisson's equation is solved to yield the potential distribution inside the device, from which the electric field can be approximated. The electric field distribution is then used in the current continuity equations to obtain the carrier distribution and the current densities. The diffusion coefficients and carrier mobilities are usually field as well as spatially dependent.

The generation-recombination term U is usually specified by the Schockley-Read-Hall relationship given below [2.12]:

$$U = Rn = \frac{pn - n_{ie}^2}{\tau_p(n + n_t) + \tau_n(p + p_t)} \tag{2.17}$$

where,

n_{ie} = Effective intrinsic carrier density.

τ_p = Hole lifetime.

τ_n = Electron lifetime.

p_t = Hole trap density.

n_t = Electron trap density.

The electron and hole mobilities are usually specified by the Scharfetter-Gummel empirical formula [2.13], as:

$$\left(\frac{\mu_0}{\mu}\right)^2 = \left[1 + \frac{N_D}{(N_D/S)+N} + \frac{(E/A)^2}{(E/A)+F} + (E/B)^2\right] \tag{2.18}$$

where,

N_D = Total ionized impurity concentration.

E = Electric field.

and N, S, A, F, and B are defined constants that have different values for electrons and holes.

2.2.1.3 Boundary Conditions

Boundary conditions have a large effect on the final solution and their specific choice is a very important issue. For ohmic contacts, infinite recombination velocities and space charge neutrality conditions are assumed [2.14]. Therefore, for a p-type material, the ohmic boundary conditions take the form:

$$V = V_{applied} + \frac{kT}{q}\ln\left(\frac{n_{ie}}{p}\right) \tag{2.19}$$

$$p = \left[\left(\frac{N_D^+ - N_A^-}{2}\right)^2 + n_{ie}^2\right]^{1/2} - \left(\frac{N_D^+ - N_A^-}{2}\right) \tag{2.20}$$

$$n = \frac{n_{ie}^2}{p} \tag{2.21}$$

where,

$V_{applied}$ = Applied voltage.

k = Boltzman's constant (1.380622×10^{-23} J/°K)

N^+_D = Ionized donor impurity concentration.

N^-_A = Ionized acceptor impurity concentration.

For Schottky contacts, the boundary conditions take the form:

$$V = V_{applied} + \frac{E_g}{2} - \phi_B \tag{2.22}$$

and

$$n = n_{ie} \exp\left(\frac{(E_g/2) - \phi_B}{kT/q}\right) \tag{2.23}$$

where,

E_g = Semiconductor bandgap.

ϕ_B = Barrier potential.

For other boundaries, across which no current must be flowing, the boundary conditions are of the form:

$$\frac{\partial V}{\partial normal} = \frac{\partial \varphi_n}{\partial normal} = \frac{\partial \varphi_p}{\partial normal} = 0 \tag{2.24}$$

where,

φ_n = Electron quasi Fermi level.

φ_p = Hole quasi Fermi level.

For Field Effect Devices, the potential under the gate may be obtained by either setting the gradient of the potential near the semiconductor-oxide interface equal to the gradient of potential inside the oxide [2.15], or by solving Laplace's equation in the oxide layer, assuming a Dirichlet boundary condition at the oxide-gate interface, and determining the potential at the semiconductor-oxide interface as:

$$\varepsilon_{SC} \left.\frac{\partial V}{\partial normal}\right|_{SC} = \varepsilon_{Ox} \frac{V_G - V_{IF}}{t} \tag{2.25}$$

where,

ε_{SC} = Permittivity of semiconductor material.

ε_{Ox} = Permittivity of the oxide.

V_G = Potential at the top of the gate.

V_{IF} = Potential of the gate near the semiconductor-oxide interface.

t = Thickness of the gate metal.

2.2.2 *Device Simulators Based on Semi-classical Approach*

The semi-classical approach is based upon the Boltzmann Transport Equation (BTE) [2.10] which can be written as:

$$\frac{df}{dt} = \frac{\partial f}{\partial t} + v \bullet \nabla_r f \pm \frac{q}{\hbar} E \bullet \nabla_k f = \left(\frac{\partial f}{\partial t}\right)_{collision} \tag{2.26}$$

where,

f = Carrier distribution function in the volume under consideration at any time t.

v = Group velocity.

E = Electric field.

q = Electronic charge.

$\hbar$ = Reduced Plank's constant.

BTE is a simplified form of the Liouville-Von Neumann equation for the density matrix. In this approach, the free flight between two consecutive collisions of the carrier is considered to be under the influence of the electric field, whereas different scattering mechanisms determine how and when the carrier will undergo a collision.

2.2.2.1 Assumptions

The assumptions for the semi-classical model can be summarized as follows:

i) Carrier to carrier interactions are considered to be very weak.

ii) Particles cannot gain energy from the electric field during collision.

iii) Scattering probability is independent of the electric field.

iv) Magnetic field effects are neglected.

v) No electron to electron interaction occurs in the collision term.

vi) Electric field varies very slowly, i.e., electric field is considered constant for a wave packet describing the particle's motion.

vii) The electron and hole gas is not degenerate.

viii) Band theory and effective-mass theorems apply to the semiconductor.

2.2.2.2 Equations to be Solved

As a starting point, Poisson's equation is solved to obtain the electric field inside the device. Using the Monte Carlo Technique (MCT) the BTE is solved to obtain the carrier distribution function, f. In the MCT, the path of one or more carriers, under the influence of external forces, is followed and from this information the carrier distribution function is determined. BTE can also be solved by the momentum and energy balance equations.

The carrier distribution function gives the carrier concentrations in the different regions of the device and can also be used to obtain the electron and hole currents, using the following expressions:

$$J_n = -q \int_k v f(r, k, t) d^3k \tag{2.27}$$

and

$$J_p = +q \int_k v f(r, k, t) d^3k \tag{2.28}$$

2.2.3 Device Simulators Based on Quantum Mechanical Approach

The quantum mechanical approach is based on the solution of the Schrödinger Wave equation (SWE) [2.16-2.19]. From equation (1.12), SWE in its time-independent form can be represented as:

$$\left(-\frac{\hbar^2}{2m^*}\nabla^2 + V\right)\psi_n(r) = E_n\psi_n(r) \tag{2.29}$$

where,

ψ_n = Wave function corresponding to the sub-band n whose minimum energy is E_n.

2.2.3.1 Equations to be Solved

In this approach, the potential distribution inside the device is calculated using Poisson's equation. This potential distribution is then used in the SWE to yield the electron wave vector which, in turn, is used to calculate the carrier distribution, using the following expression:

$$n = \sum_{n} N_n |\psi_n|^2 \tag{2.30}$$

where,

n = carrier concentration.

N_n = Number of allowed states in the sub-band n.

This carrier concentration is again used in Poisson's equation and a new set of ψ_n, E_n, and n is calculated. This process is repeated until a self-consistent solution is obtained. The final wave vector is invoked to determine the scattering matrix following which MCT is used to yield the carrier distribution and current densities.

2.2.4 Commercially Available Device Simulation Packages

The classical approach is the most commonly used procedure since it is the easiest to implement and, in most cases, the fastest technique. Simulators based on the classical

approach are available in two-dimensional forms like FEDAS [2.20], HESPER [2.20], PISCES-II [2.21], PISCES-2B [2.22], MINIMOS [2.23], BAMBI [2.24] or three dimensional like TRANAL [2.20], SIERRA [2.25], FIELDAY [2.20], DAVINCI [2.22], CADDETH [2.26].

Large dimension devices, where the carriers travel far from the boundaries, can be simulated based on a one-dimensional approach. However most currently-used devices do not fit into this category and therefore one has to resort to either two- or three-dimensional simulators.

FEDAS (Field Effect Device Analysis System) is a two dimensional device simulator that simulates MOSFET's, JFET's and MESFET's by considering only those carriers that form the channel. The Poisson equation is solved everywhere except in the oxide region. Instead of carrying the potential calculation within the oxide region, the potential at the semiconductor-oxide interface is calculated by assuming a mixed boundary condition. FEDAS uses FDM (Finite Difference Method) to solve the set of linear equations. A three-dimensional variation of FEDAS is available for the simulation of small geometry MOSFETs.

HESPER (HEterostructure device Simulation Program to Estimate the performance Rigorously) is a two-dimensional device simulator which can be used to simulate

heterostructure photodiodes, HBTs, and HEMTs. The simulation starts with the solution of Poisson's equation in which the electron and hole concentrations are described as functions of the composition (composition dependent). The recombination rate is given by the Schockley-Read-Hall. Lifetimes of both types of carriers are assumed to be equal in this model.

PISCES-2B is a two-dimensional device simulator for simulation of diodes, BJTs, MOSFETs, JFETs, and MESFETs. Besides steady-state analysis, transient and AC small-signal analysis can also be performed.

2.3 Solution Methods

The partial differential equations encountered in the simulation of semiconductor devices, may be solved by either the Finite Difference Method (FDM) [2.27, 2.28] or the Finite Element Method (FEM) [2.29- 2.32]. Recently Boundary Element Method (BEM) has also been applied to the solution of these equations [2.33-2.35].

In FDM, the region under simulation is divided into rectangular or triangular areas for two dimensional cases, or into cubic or tetrahedron volumes in three-dimensional cases. Each corner or vertex is considered as a node. The differential equations are modified using Finite Difference Approximations, and a set of equations is constructed in matrix

form. The finite difference approximations are obtained from Taylor series expansion of the function around the simulation point. When the system of equations is written in the matrix form, the resulting matrix can be made highly sparse. Considerable computational efficiency can be gained by taking advantage of the sparsity of the matrix. The Finite Difference Equations are solved iteratively at only these non-zero nodes. The most commonly used solvers are Gauss-Seidel/Jacobi (G-S/J) techniques or Newton's Technique (NT) [2.36]. FDM has the disadvantage of requiring more nodes than the FEM for the same structure. However a new variation of FDM, namely the Finite Boxes Scheme [2.37], overcomes this problem by enabling local area refinement. The advantage of FDM is that its computational memory requirement is less than that required for FEM due to the band structure of the matrix.

FEM was developed in the early 1950s to solve problems related to mechanics of deformable continuous media. The method has evolved considerably and is now frequently applied to boundary value problems such as the those involved in semiconductor device simulation. In FEM, the region under simulation is divided into triangular and quadrilateral regions in two dimensions or into tetrahedra in three dimensions. The regions are placed so as to have the maximum number of vertices in areas where there is expected to be a large variation of composition or a large variation in the solution. The equations in FEM are modified by multiplying them with a shape function and integrating over the simulated region. In triangular meshes, the shape

function is dependent on the area of the triangle and the spatial location of the node. The value of the spatial function is between 0 and 1. The solution at one node is the sum of all the solutions, resulting from the nearby nodes, multiplied by their respective shape functions. The number of nodes required to simulate a region is less than that in FDM, however the memory requirement is greater.

BEM has not been very actively used in semiconductor device solution due to the non-linearity of the exponential functions encountered [2.35]. BEM is a boundary integral method, where the simulation domain is defined on all boundaries. The solution of the equations on the boundary is extrapolated to the interior, thus obtaining a solution of the differential equation in the complete domain. BEM methods usually do not resort to gridding of the domain, therefore they are very efficient in computer resource utilization. However, the preprocessing of the differential equations to make them suitable for BEM methods and the extreme care required in treating the exponential functions have impeded the acceptance of this method by the semiconductor device simulation community.

Chapter 3

Description of the Technical Problem

As pointed out in the previous chapter, both the classical and the semi-classical approaches are reached after making certain assumptions about the transport behavior of the charged carriers [2.10].

In this chapter, sections 3.1 and 3.2 present the assumptions taken in deriving the necessary transport equations. The effects of these assumptions are also discussed and the validity of using the quantum mechanical approach is thus shown in section 3.3.

3.1 Semi-classical Approach

Starting from a quantum mechanical view of materials, the semi-classical approach can be obtained with appropriate assumptions. The semi-classical approach is based on the transport equation approach, which describes the probability of finding a carrier in a given energy state [3.1]. Starting from a quantum mechanical picture, one can deduce the transport equation for any distribution function [3.2, 3.3].

In order to determine Boltzmann's transport equation [2.2], one can assume,

$n(k,r,t)$ = Density of carriers.

$f(k,r,t)$ = Distribution function.

where,

(k,r,t) = Represent momentum, Cartesian, and temporal space coordinates, respectively.

One can relate the particle density to the distribution function as,

$$n(r,t) = \int f(k,r,t)dk, \qquad \text{over all } k \text{ space} \tag{3.1}$$

The probability that the carrier exists along the trajectory r,k always exists. Therefore, the distribution function does not change along this trajectory as time goes by. Thus,

$$\frac{df(k,r,t)}{dt} = 0 \tag{3.2}$$

Denoting $f(k,r,t)$ by f, and expanding the time derivative of the distribution function, one can get.

$$\frac{df}{dt} = \frac{\partial f}{\partial t} + \frac{\partial f}{\partial r} \bullet \frac{\partial r}{\partial t} + \frac{\partial f}{\partial k} \bullet \frac{\partial k}{\partial t} = 0 \tag{3.3}$$

If a force is made to act on a particle, it will cause the carrier's momentum to change, one can represent this force by,

$$F_{total} \propto \frac{dk}{dt} \tag{3.4}$$

or,

$$F_{total} = \hbar \frac{dk}{dt} \tag{3.5}$$

where,

F_{total} = Total force acting on the carrier.

If the only external force acting on the carrier is the external electric field, and the only internal force acting on the carrier is due to collision with other carriers then,

$$F_{total} = F_{internal} + F_{external} \tag{3.6}$$

where,

$$F_{external} = \pm qE \tag{3.7}$$

and,

E = External electric field.

$\pm q$ = Charge of an electron or a hole.

Furthermore, one can describe the group velocity, v, of the carriers as,

$$v = \frac{dr}{dt} \tag{3.8}$$

Therefore after substituting equations (3.5), (3.6), (3.7), and (3.8) in equation (3.3) one can arrive at the familiar form of the Boltzmann's transport equation.

$$\frac{\partial f}{\partial t} + v \bullet \nabla_r f \pm \frac{q}{\hbar} E \bullet \nabla_k f = \left(\frac{\partial f}{\partial t}\right)_{collision} \tag{3.9}$$

The assumptions made to derive the Boltzmann's transport equation can be summerized as follows:

i) *Carrier to carrier interactions are considered to be very weak.*

In the quantum mechanical picture, the carrier wave function has the property of interaction with itself as well as with other carriers. However, in the semi-classical approach, the transport is assumed to be single particle and as such no other carriers or their interaction is assumed.

ii) *Particles cannot gain energy from the electric field during collision.*

It is assumed that between collisions the particle cannot gain energy from the electric field. All collisions are assumed to be elastic.

iii) *Scattering probability is independent of the electric field.*

Electric field does not influence the scattering probability. This is due to the fact that the forces acting on the particle are considered to be external and internal and there is no interaction between the two terms.

iv) *Magnetic field effects are neglected.*

No magnetic field is assumed. The external force acting on the particle is entirely electric.

v) *No electron to electron interaction occurs in the collision term.*

Scattering is assumed to be due to the collision of the transport particle with other non transport particles.

vi) *Electric field varies very slowly, i.e., electric field is considered constant for a wave packet describing the particle's motion.*

Electric field acting on the particle is assumed to be constant for the duration of the mean free path.

vii) *The electron and hole gas is not degenerate.*

The quantum mechanical interactions of the carriers, due to degeneracy, are not considered in this approach.

viii) *Band theory and effective-mass theorems apply to the semiconductor.*

The perturbation due to the periodic potential of the crystalline structure is compensated by the introduction of the effective mass concept.

3.2 Classical Approach

In order to develop the classical approach, this time one can start from Boltzmann's transport equation previously derived. Rewriting the Boltzmann's transport equation in the momentum conservation form,

$$\frac{\partial v}{\partial t} + v \bullet \nabla_r v \pm \frac{qE}{m^*} - \frac{kT_e}{m^* n}\nabla_r n - \frac{k}{m^*}\nabla_r T_e = \left(\frac{\partial v}{\partial t}\right)_{collision} \tag{3.10}$$

where,

v = Carrier velocity.

m^* = Effective mass of the carrier.

n = Carrier distribution.

T_e = Carrier Temperature.

k = Boltzmann's constant.

E = Electric field.

q = Electronic charge.

The current continuity equations for the classical approach can be obtained by making the following approximations to the momentum conservation form of the Boltzmann's Transport Equation:

i) *Carrier temperature is the same throughout the device and is assumed to equal the lattice temperature.*

This assumption is the same as assuming that no carrier-phonon interaction takes place. Due to this assumption, one can write,

$$\nabla_r T_e = \nabla_r T = 0 \tag{3.11}$$

where,

T_e = Carrier temperature, and

T = Lattice temperature.

ii) *Quasi steady-state conditions exist.*

Since there is an order of magnitude difference between the response time of the device and the circuit, therefore a quasi steady-state model is sufficient, thus;

$$\frac{\partial v}{\partial t} = 0 \tag{3.12}$$

iii) *Carrier mean free path must be smaller than the distance over which the quasi Fermi level is changing by kT/q.*

The quasi Fermi levels do not change during the mean free path of the carrier. Thus, the carrier does not alter its energy state between collisions.

iv) *The impurity concentration is constant or varies very slowly along the mean free path of the carrier.*

No abrupt changes in the impurity concentration are assumed while the carrier is in free flight.

v) *Energy band is parabolic.*

This assumption assures that the effective mass concept applied due to the periodicity of the crystalline structure is still valid.

vi) *Influence of the boundary conditions is negligible.*

The area of interest in the simulated device is placed far enough from the boundaries, so as to ensure that the boundary conditions do not influence the solution in that area.

vii) *Carrier velocity does not vary significantly over the mean free path of the carrier.*

Thus,

$$v \bullet \nabla_r v \approx 0 \tag{3.13}$$

Substituting equations (3.11), (3.12), and (3.13) in equation (3.10), one can get;

$$-\frac{qE}{m^*} - \frac{kT}{m^* n}\nabla_r n = \left(\frac{\partial v}{\partial t}\right)_{collision} = \frac{v_n}{\tau_n} \tag{3.14}$$

where,

v_n = Carrier velocity (in this case electron velocity).

τ_n = Mean free time between collisions.

Rearranging equation (3.14) gives;

$$v_n = -\frac{\tau_n qE}{m^*} - \frac{kT}{m^* n}\tau_n \nabla_r n \tag{3.15}$$

Using expressions for electron mobility, μ_n, and diffusion coefficient, D_n;

$$\mu_n = \frac{q\tau_n}{m^*} \tag{3.16}$$

and

$$D_n = \frac{kT\tau_n}{m^*} \tag{3.17}$$

One can write equation (3.15) as,

$$v_n = -\mu_n E - \frac{D_n}{n}\nabla_r n \tag{3.18}$$

Defining,

$$J_n = -qnv_n \tag{3.19}$$

This enables one to write equation (3.18) in the familiar current continuity form as,

$$J_n = qn\mu_n E + qD_n \nabla_r n \tag{3.20}$$

A similar expression can be written for the hole current density.

$$J_p = qp\mu_p E - qD_p \nabla_r p \tag{3.21}$$

3.3 Choice of Quantum Mechanical Approach

The Boltzmann's transport equation does not take into account the finite duration of the scattering process [3.4]. In the BTE it is assumed that the collisions are instantaneous, however in small geometry semiconductor devices, under strong electric fields, the collisions are not instantaneous and thus the transport behavior must be modified. Furthermore, very high concentration systems are not modeled accurately in the BTE approach. The interaction of carriers among themselves is assumed to be very weak. Only interaction with other non carriers is assumed. Thus BTE, cannot provide accurate

picture for devices where the current is carried by both type of carriers, and where the interaction between same type of carriers produces non classical effects, e.g., formation of allowed energy band due to interaction of the wave function of the carriers.

In the same way, the classical approach based on the solution of current continuity equation also does not provide a complete and accurate picture of small geometry devices and hot electron effects.

Therefore, in order to provide an accurate response of a semiconductor device, a quantum mechanical approach must be considered. This is true especially for very small geometry devices and devices with complex structures, e.g., quantum well structures.

Chapter 4

Solution Method Based on Quantum Mechanical Approach

The simulation approach used in this work is based on the self consistent solution of the Poisson and the time independent Schrödinger wave equations. The two equations are given by (1.12) and (1.20) and reproduced here again.

$$E\psi(r) = -\frac{\hbar^2}{2m^*}\nabla^2\psi(r) + V\psi(r) \tag{4.1}$$

and

$$\nabla \bullet (\varepsilon E) = q_{ev} \tag{4.2}$$

One can rewrite equations (4.1) and (4.2) in the more familiar one dimensional forms as,

$$\left(-\frac{\hbar^2}{2m^*(i)}\nabla^2 + V(i)\right)\psi(i) = E_\lambda\psi(i \tag{4.3}$$

and

$$\nabla \bullet [\varepsilon_0\varepsilon_r(i)\nabla V(i)] = -q[N_D^+(i) - n(i) + p(i) - N_A^-(i) \tag{4.4}$$

In equation (4.3), the input parameters are,

$m^*(i)$ = Effective mass of the carrier.

$V(i)$ = Potential inside the simulation region.

The ∇^2 operator is computed based on the mesh gridding data.

Equation (4.3) is solved to obtain the eigen value, E_λ, and the corresponding eigen vectors, $\psi(i)$.

In equation (4.4), the input parameters are,

$\varepsilon_r(i)$ = Relative permittivity of the material.

$N^+_D(i)$ = Ionized donor impurity concentration.

$n(i)$ = Electron concentration.

$p(i)$ = Hole concentration.

$N^+_A(i)$ = Ionized acceptor impurity concentration.

Equation (4.4) is solved to obtain the potential inside the simulation region, $V(i)$.

The constants used in the two equation are $\hbar$, ε_0, and q which are the reduced Planck's constant, permittivity of free space, and the electronic charge, respectively.

4.1 Parameter Input and Grid Calculation

Due to the simplicity of formulation of the equations, it was decided to solve equations (4.3) and (4.4) using finite difference method. The finite difference formulation is based on the unequal grid spacing so as to be able to refine the grid in areas of interest. Due to complex nature of the devices, it becomes essential that the regions of rapidly varying characteristics be finely meshed to reduce error and increase smoothness of the solution.

The different parameters required for the simulation of the device are read from an input file. These parameters are

i) Gridding information, $x(i)$.

ii) Operating temperature of the device, T.

iii) Error criteria, e_{max}.

iv) Relative permittivity, $\varepsilon_r(i)$.

v) Initial potential estimate, $V(i)$.

vi) Longitudinal and transverse electron masses, $m_l^*(i)$ and $m_t^*(i)$, respectively.

vii) Light and heavy hole masses, $m_{lh}^*(i)$ and $m_{hh}^*(i)$, respectively.

viii) Donor and acceptor impurity concentrations, $N_D(i)$ and $N_A(i)$.

ix) Donor and acceptor ionization energies, E_D, E_A.

x) Bandgap at *0* °K, $E_g(0)$.

xi) Bandgap temperature dependent parameters, α and β.

xii) Electron affinity, χ.

xiii) Number of minima of the conduction band, M_C.

The operating temperature is used to compute the bandgap in the different regions of the device, using [4.3];

$$E_g(T) = E_g(0) - \frac{\alpha T^2}{(T+\beta)} \tag{4.5}$$

Using $E_g(T)$ and χ, the conduction and valence band energies, $E_C(i)$ and $E_V(i)$ are computed. An arbitrary value for the vacuum level (10.0 eV in this case) is chosen. Since the conduction and valence band energies are normalized with respect to the Fermi energy levels, therefore the choice of the vacuum energy level is not critical. Hence, before normalization, the conduction and valence band energies are,

$$E_C(i) = 10.0 - \chi \tag{4.6}$$

and

$$E_V(i) = 10.0 - \chi - E_g(T) \tag{4.7}$$

Conduction and valence band offsets, ΔE_C and ΔE_V, resulting at the heterointerface, are also calculated. These offsets are based on the difference in the electron affinities of

the adjacent regions. The values of the conduction and valence band offsets calculated in this way agree well with the experimentally measured values [4.2].

4.2 Fermi Energy Calculation

Before Fermi energy is calculated, the electron and hole effective masses and the conduction and valence band density of states are calculated. The effective masses are given by,

$$m_e^* = \left(m_l^* \times (M_C \times m_t^*)^2 \right)^{1/3} \tag{4.8}$$

$$m_h^* = \left[(m_{lh})^{3/2} + (m_{hh})^{3/2} \right]^{2/3} \tag{4.9}$$

and the conduction and valence band density of states are given by,

$$N_C = 2\left[\frac{m_e^* kT}{2\pi\hbar^2} \right]^{3/2} \tag{4.10}$$

$$N_V = 2\left[\frac{m_h^* kT}{2\pi\hbar^2} \right]^{3/2} \tag{4.11}$$

Fermi energy of each region is calculated using the charge neutrality condition. According to the charge neutrality condition, under equilibrium,

$$(N_D^+ - n + p - N_A^-) = 0 \tag{4.12}$$

Equation (4.12) can be solved by substituting,

$$N_D^+ = \frac{N_D}{1 + g_D exp\left(\frac{E_F - E_D}{kT}\right)} \tag{4.13}$$

where,

g_D = Spin degeneracy (usual value is 2).

$$N_A^- = \frac{N_A}{1 + g_A exp\left(\frac{E_A - E_F}{kT}\right)} \tag{4.14}$$

where,

g_A = Light and heavy hole degeneracy (usual value is 4).

$$n = N_C exp\left(\frac{-(E_C - E_F)}{kT}\right) \tag{4.15}$$

$$p = N_V exp\left(\frac{(E_V - E_F)}{kT}\right) \tag{4.16}$$

If one can denote,

$$E_C - E_F = X \tag{4.17}$$

then, by substituting equation (4.17) in equations (4.13 - 4.16) and using the results in equation (4.12) one can get,

$$\frac{N_D}{1+g_D exp\left(\frac{-X+E_D}{kT}\right)} - N_C exp\left(\frac{-X}{kT}\right) + N_V exp\left(\frac{(X-E_g)}{kT}\right) - \frac{N_A}{1+g_A exp\left(\frac{X+E_A-E_g}{kT}\right)} = 0 \tag{4.18}$$

Equation (4.18) is solved for X, which is a root of this equation, using the bisection method. The root is then further refined using Newton's method.

Once Fermi level for each region has been computed, then using equations (4.13 - 4.16) the ionized impurity concentrations as well as the electron and hole concentrations are computed.

4.3 Poisson Equation Solution

The Poisson equation is discritized using the central differenced formula. The central differenced formula is based on the second order accurate Taylor series approximation.

Reproducing equation (4.2),

$$\nabla \bullet [\varepsilon_0 \varepsilon_r(i) \nabla V(i)] = -q[N_D^+(i) - n(i) + p(i) - N_A^-(i) \tag{4.19}$$

For a heterostructure with varying relative permittivity, equation (4.19) can further be expanded to yield,

$$\nabla^2 V(i) + \frac{1}{\varepsilon_r(i)} \nabla \varepsilon_r(i) \bullet \nabla V(i) = -\frac{q[N_D^+(i) - n(i) + p(i) - N_A^-(i)}{\varepsilon_o \varepsilon_r(i)} \tag{4.20}$$

Using the second order central differenced approximation;

$$\nabla^2 V(i) = \frac{\frac{V(i+1)-V(i)}{\Delta X_{i+1,i}} - \frac{V(i)-V(i-1)}{\Delta X_{i,i-1}}}{(1/2)(\Delta X_{i+1,i} + \Delta X_{i,i-1})} \tag{4.21}$$

where,

$$\Delta X_{i+1,i} = x(i+1) - x(i) \tag{4.22}$$

$$\Delta X_{i,i-1} = x(i) - x(i-1) \tag{4.23}$$

Using second order forward differenced approximation;

$$\nabla \varepsilon_r(i) = \frac{\varepsilon_r(i+1) - \varepsilon_r(i-1)}{(\Delta X_{i+1,i} + \Delta X_{i,i-1})} \tag{4.24}$$

and

$$\nabla V(i) = \frac{V(i+1) - V(i-1)}{(\Delta X_{i+1,i} + \Delta X_{i,i-1})} \tag{4.25}$$

In order to solve equation (4.20), appropriate boundary conditions are required. When solving for the potential inside the device, there are two types of boundary conditions that may be used. At boundaries where the potential is invariable, Dirichlet boundary condition is used, while at boundaries across which no current must flow, Neumann boundary condition is used. Neumann boundary condition may also be defined as zero electric field boundary condition. The Dirichlet boundary condition may be represented as,

$$|V(i)|_{Boundary} = V_{Fixed} \tag{4.26}$$

The Neumann boundary condition may be derived using an interpolating polynomial. In this case, a second order accurate Newton polynomial of degree 2 is used. Consider three points at the boundary, Figure 4.1. One can develop a polynomial passing through these points, using the Newton's divided difference formula [4.3].

Thus,

$$P_2(x) = f[x_1] + f[x_1, x_2](x - x_1) + f[x_1, x_2, x_3](x - x_1)(x - x_2) \tag{4.27}$$

where,

$$f[x_1] = f(x_1) \tag{4.28}$$

$$f[x_1, x_2] = \frac{f(x_2) - f(x_1)}{(x_2 - x_1)} \tag{4.29}$$

$$f[x_1, x_2, x_3] = \frac{f(x_3) - f(x_1) - \frac{f(x_2) - f(x_1)}{(x_2 - x_1)}(x_3 - x_1)}{(x_3 - x_1)(x_3 - x_2)}(x - x_1)(x - x_2) \tag{4.30}$$

According to the Neumann boundary condition, the derivative of the function, $V(i)$ in this case, must go to zero at the boundary. Therefore, substituting equations (4.28 - 4.30) in equation (4.27) and differentiating the resulting equation and forcing the differential to go to zero at x_1, gives $V(x_1)$ as,

$$V(x_1) = \frac{V(x_2)\left[\frac{1}{\Delta X_{2,1}} + \frac{1}{\Delta X_{3,2}}\right] + V(x_3)\left[\frac{-1}{\Delta X_{3,2}} + \frac{1}{\Delta X_{3,1}}\right]}{\left[\frac{1}{\Delta X_{2,1}} + \frac{1}{\Delta X_{3,1}}\right]} \tag{4.31}$$

A similar expression for zero differential at x_3, gives $V(x_3)$ as,

$$V(x_3) = \frac{V(x_2)\left[\frac{1}{\Delta X_{2,1}} + \frac{1}{\Delta X_{3,2}}\right] + V(x_1)\left[\frac{-1}{\Delta X_{2,1}} + \frac{1}{\Delta X_{3,1}}\right]}{\left[\frac{1}{\Delta X_{3,2}} + \frac{1}{\Delta X_{3,1}}\right]} \tag{4.32}$$

The Neumann boundary condition is direction dependent, therefore equation (4.31) is used at the $x=0$ while equation (4.32) is used at $x=n$.

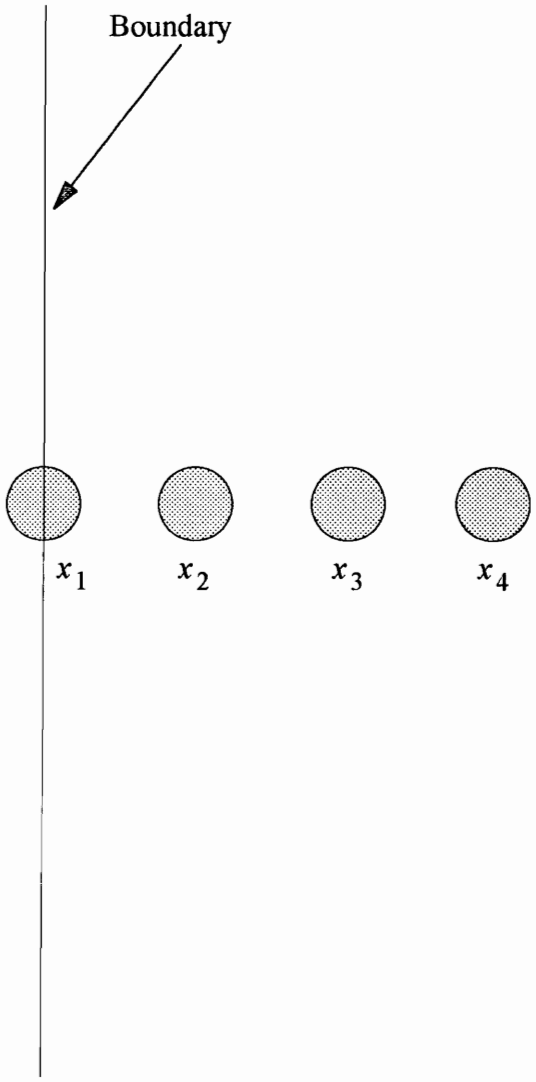

Figure 4.1, Boundary Points for Neumann Polynomial

Thus, there are two solution regimes, one exclusively at the boundaries and the other exclusively inside the domain of the device. With these approximations, the equation to be solved exclusively inside the simulation domain becomes,

$$V(i) = \frac{V(i+1)[Term_{i+1}] + V(i-1)[Term_{i-1}] + [Rho_i]}{[Term_i]} \tag{4.33}$$

where,

$$Term_{i+1} = \left[\frac{2}{\Delta X_{i+1,i}(\Delta X_{i+1,i} + \Delta X_{i,i-1})} + \frac{(\varepsilon_{r_{i+1}} - \varepsilon_{r_{i-1}})}{\varepsilon_{r_i}(\Delta X_{i+1,i} + \Delta X_{i,i-1})^2} \right] \tag{4.34}$$

$$Term_{i-1} = \left[\frac{2}{\Delta X_{i,i-1}(\Delta X_{i+1,i} + \Delta X_{i,i-1})} - \frac{(\varepsilon_{r_{i+1}} - \varepsilon_{r_{i-1}})}{\varepsilon_{r_i}(\Delta X_{i+1,i} + \Delta X_{i,i-1})^2} \right] \tag{4.35}$$

$$Term_i = \left[\frac{2}{\Delta X_{i+1,i}(\Delta X_{i+1,i} + \Delta X_{i,i-1})} + \frac{2}{\Delta X_{i,i-1}(\Delta X_{i+1,i} + \Delta X_{i,i-1})} \right] \tag{4.36}$$

$$Rho_i = \frac{q[N_D^+(i) - n(i) + p(i) - N_A^-(i)]}{\varepsilon_o \varepsilon_r(i)} \tag{4.37}$$

At the boundaries, either the Dirichlet or the Neumann conditions are solved. These equations are given by equations (4.26), (4.31) and (4.32). In the cases where only Neumann boundary condition is used, the potential inside the device still needs to be pinned down to obtain a converging solution. Pinning down of the solution of Poisson equation does not effect the solution of Schrödinger equation, since the potential is

normalized to the Fermi level before being applied in the Schrödinger equation. Thus, the solution can be arbitrarily pinned down at any point to any potential value.

4.4 Energy Band Normalization

The potential profile obtained from the solution of the Poisson's equation is flipped, since the conduction band varies as a mirror image of the built-in potential, and set equal to the conduction band profile. The conduction band profile is normalized to zero. The minima of the conduction band profile is determined and the fermi level at that point is taken as the base fermi level. This base fermi level is added to the conduction band profile to obtain the conduction band energy.

A similar technique is used for the valence band profile. First the valence band profile is computed by using the band gap information and the potential distribution obtained from the Poisson's equation. The Fermi-Dirac distribution function for holes assumes that the valence band will lie below the fermi level, therefore the eigen values obtained will have negative signs. The carrier concentration formulas that will be used employ a root of the eigen value, thus rendering the conduction band approach of flipping the potential as inappropriate. Therefore in this case, the valence band is taken to lie above the fermi level. The maxima of the computed valence band is determined and the fermi level of the

corresponding point is assumed as the base fermi level for the valence band. The valence band is then normalized to the valence band base fermi level.

The minimum and maximum of E_C and E_V are also computed. These limits are used to determine the valid eigen values, since all valid eigen values of interest will lie within these limits.

4.5 Schrödinger Wave Equation Solution

The Schrödinger wave equation is also discritized using a second order accurate central differenced approximation for the second order derivative. The Schrödinger wave equation is given by equation (4.1) and reproduced here.

$$\left(-\frac{\hbar^2}{2m^*(i)}\nabla^2 + V(i)\right)\psi(i) = E_\lambda \psi(i) \tag{4.38}$$

For a heterostructure with varying carrier mass, equation (4.38) can be rewritten as,

$$-\frac{\hbar^2}{2}\left(\nabla \bullet \frac{1}{m^*(i)}\nabla\psi(i)\right) + V(i)\psi(i) = E_\lambda \psi(i) \tag{4.39}$$

In its discritized form, equation (4.39) may be written as,

$$-\frac{\hbar^2}{2}\left[\frac{\frac{1}{m^*(i+1/2)}\frac{\psi(i+1)-\psi(i)}{\Delta X_{i+1,i}}-\frac{1}{m^*(i-1/2)}\frac{\psi(i)-\psi(i-1)}{\Delta X_{i,i-1}}}{(1/2)(\Delta X_{i+1,i}+\Delta X_{i,i-1})}\right]+V(i)\psi(i)=E_\lambda\psi(i) \qquad (4.40)$$

Equation (4.40) is an eigen value problem, with E_λ and $\psi(i)$ as the two unknowns. We can write equation (4.40) in matrix form as,

$$A\psi = E_\lambda\psi \qquad (4.41)$$

For a one dimensional case A is a tri-diagonal matrix, with the following elements.

$$L=\frac{-\hbar^2}{m^*_{i-1/2}\Delta X_{i,i-1}(\Delta X_{i+1,i}+\Delta X_{i,i-1})} \qquad \text{for } i>1 \qquad (4.42)$$

$$D=\frac{\hbar^2}{m^*_{i+1/2}\Delta X_{i+1,i}(\Delta X_{i+1,i}+\Delta X_{i,i-1})}+\frac{\hbar^2}{m^*_{i-1/2}\Delta X_{i,i-1}(\Delta X_{i+1,i}+\Delta X_{i,i-1})} \qquad \text{for } i=1,\ldots,n \qquad (4.43)$$

$$U=\frac{-\hbar^2}{m^*_{i+1/2}\Delta X_{i+1,i}(\Delta X_{i+1,i}+\Delta X_{i,i-1})} \qquad \text{for } i<n \qquad (4.44)$$

Observing equations (4.42 - 4.44), it becomes clear that for a non uniform grid the lower and the upper diagonal elements will not be equal. Thus, destroying the symmetricity of the matrix and resulting in a tedious solution of the eigen value problem. In order to improve the efficiency of the eigen value solver, the symmetricity of the

resulting matrix is restored by preconditioning the A matrix [2.25] by a diagonal matrix. The diagonal elements of the preconditioning matrix are given by,

$$X_p = \frac{1}{(\Delta X_{i+1,i} + \Delta X_{i,i-1})} \tag{4.45}$$

Equation (4.41) thus becomes,

$$(X_p)A' \psi = E_\lambda \psi \tag{4.46}$$

Observing A', it becomes clear that it is symmetric even for non uniform gridding. This system of matrix may also be written as,

$$\sqrt{(X_p)}\ \sqrt{(X_p)}\ A' \psi = E_\lambda \psi \tag{4.47}$$

Since,

$$\sqrt{(X_p)}\ \sqrt{(X_p)}^{-1} = \text{Identity matrix} \tag{4.48}$$

Therefore, one can multiply both sides of equation (4.47) by equation (4.48) and $\sqrt{(X_p)}^{-1}$

This gives equation (4.47) as,

$$\sqrt{(X_p)}^{-1}\sqrt{(X_p)}\sqrt{(X_p)}A'\sqrt{(X_p)}\sqrt{(X_p)}^{-1}\psi = E_\lambda\sqrt{(X_p)}^{-1}\sqrt{(X_p)}\sqrt{(X_p)}^{-1} \quad (4.49)$$

Equation (4.49) can thus be simplified to,

$$\sqrt{(X_p)}A'\sqrt{(X_p)}\sqrt{(X_p)}^{-1}\psi = E_\lambda\sqrt{(X_p)}^{-1}\psi \quad (4.50)$$

If one can represent,

$$A'' = \sqrt{(X_p)}A'\sqrt{(X_p)}$$

and,

$$\Psi = \sqrt{(X_p)}^{-1}\psi$$

Then, the matrix system becomes,

$$A''\Psi = E_\lambda\Psi \quad (4.51)$$

Here, A'' is still a real symmetric tri-diagonal matrix, and the eigen vectors can be obtained using the relation,

$$\psi = \sqrt{(X_p)}\Psi \quad (4.52)$$

4.6 Probability Function Check

The probability function for the domain *dx*, is defined as,

$$\int \psi(i)^* \psi(i) dx = 1 \tag{4.53}$$

where,

$\psi(i)^*$ = Conjugate of $\psi(i)$.

Probability function defines the probability of finding a particle anywhere in the domain of the wave function as being equal to 1. Now since the eigen value matrix system was preconditioned to maintain matrix symmetricity, therefore the eigen vectors obtained as the solution of that system are normalized with respect to the preconditioning matrix. Therefore in order to satisfy equation (4.53), the eigen vectors need to be normalized again. In fact it is found that the original eigen vector, Ψ, obtained from the solution of equation (4.51) is the normalized eigen vector. The eigen vector, Ψ, is then substituted instead of, ψ, in the carrier concentration equations [4.4].

4.7 Carrier Concentration Calculation

The wave vector and the eigen energy value are then be used to determine the carrier concentration. Since the parameters and device itself are three dimensional (since, in a

one dimensional simulation one is only observing the system variations in one dimension of a three dimension system), therefore this approach uses a single dimension version of the three dimensional density of state function. In order to derive such a function, it is assumed that there is a three dimensional space, with volume Ω, as shown in Figure 4.2(a). Assuming that a carrier of one particular energy occupies a rectangular space, *abc*, Figure 4.2(b). Now, looking at the domain in reciprocal space, then each spatial coordinate can be defined as,

$$k_x = \frac{\pi}{a} \tag{4.54}$$

$$k_y = \frac{\pi}{b} \tag{4.55}$$

$$k_z = \frac{\pi}{c} \tag{4.56}$$

where,

k_x, k_y, and k_z are the three components of the k-state vector, k, such that,

$$k^2 = k_x^2 + k_y^2 + k_z^2 \tag{4.57}$$

Therefore, the total number of k-states in the volume, Ω, is given by,

$$\frac{\Omega}{(k_x k_y k_z)} = \frac{\Omega}{(\pi^3/abc)} = \frac{\Omega a}{\pi^3} \tag{4.58}$$

where, it has been assumed that b and c have unit lengths.

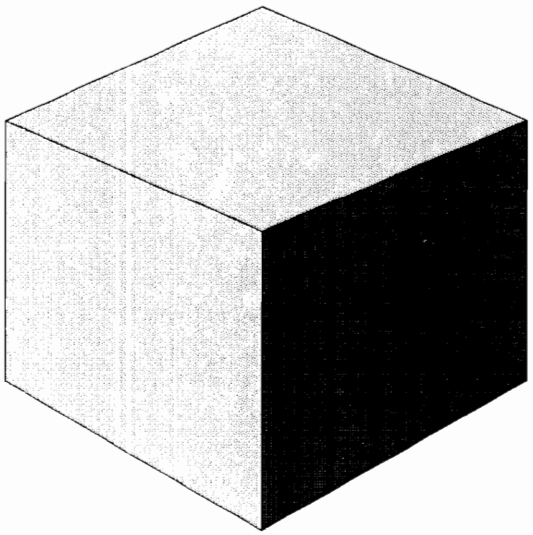

(a) Three Dimensional Space with Volume Ω

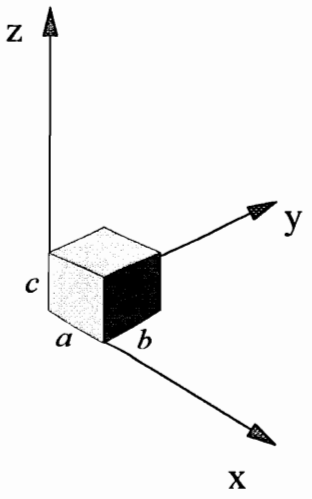

(b) Rectangular Space, *abc*, Occupied by a Carrier

Figure 4.2

Since k comprises of $\pm k_x$, $\pm k_y$, $\pm k_z$, therefore there is a redundancy of 8 in the solution for a particular energy state. Thus the total number of k-states is reduced by a factor of 8 for three dimensional systems. Now since each energy state can be occupied by two electrons of opposite spin, therefore the k-states are also multiplied by 2. Therefore actual number of k-states in the volume, Ω, is given by,

$$\frac{\Omega}{4\pi^3 a} \tag{4.59}$$

Therefore, number of k-states per unit volume is given by,

$$\frac{a}{4\pi^3} \tag{4.60}$$

and the density of k-states per unit volume becomes,

$$\frac{1}{4\pi^3} \tag{4.61}$$

Now assume that the carrier has some energy, E. In its ground state this carrier cannot posses energy more than the fermi energy E_F. We can represent E_F in reciprocal space by a vector of length k_F. Thus the carrier will be bounded in reciprocal space by a sphere of volume,

$$\frac{4\pi}{3} k_f^3 \tag{4.62}$$

If the energy of the particle is increased, or correspondingly the volume of the k-space sphere is increased from k to $k+dk$, then the increase in the k-space spherical volume is given by,

$$4\pi k^2 dk \tag{4.63}$$

where, it has been assumed that, $dk << k$ and $dk << 1$.

Therefore the excess density of k-states per unit volume, is now given by,

$$\frac{1}{4\pi^3} \times 4\pi k^2 dk = \frac{k^2}{\pi} dk = \frac{k_x^2}{\pi} dk_x + \frac{k_z^2}{\pi} dk_y + \frac{k_z^2}{\pi} dk_z \tag{4.64}$$

Assuming that y and z direction density of states are the same as x direction density of state, therefore one can write equation (4.64) as,

$$\frac{k_x^2}{\pi} dk_x = \frac{k^2}{3\pi} dk \tag{4.65}$$

Representing k and dk by their energy equivalencies,

$$k^2 = \frac{2m^* E}{\hbar^2} \tag{4.66}$$

and

$$dk = \frac{1}{2} \frac{\sqrt{2m^*}}{\hbar} E^{-1/2} dE \tag{4.67}$$

Therefore the total number of energy states between E and $E+dE$, for a single dimension of a three dimensional system is given by,

$$N(E) = \frac{\sqrt{2}\, m^{*3/2}}{3\pi^2\hbar^3} E^{1/2} dE \tag{4.68}$$

The probability that an energy state is occupied is given by the distribution function. There are three types of distribution functions, Maxwell-Boltzmann, Fermi-Dirac, and Bose-Einstein. In this work, the Fermi-Dirac distribution function is used. As explained in section 4.4, the Fermi-Dirac distribution function for electrons as well as holes is given by,

$$f(E) = \frac{1}{1 + \exp\left(\frac{E-E_F}{kT}\right)} \qquad \text{for electrons and holes} \tag{4.69}$$

The electron concentration for each eigen energy state, n_λ, for a one-dimensional case, is therefore given by,

$$n_\lambda = \frac{\sqrt{2}\, m^{*3/2}}{3\pi^2\hbar^3} \int_{E_\lambda}^{\infty} \frac{E^{1/2}}{1 + exp\left(\frac{E-E_F}{kT}\right)} dE \tag{4.70}$$

The upper integration limit can safely be replaced by some higher energy level, without much loss of accuracy, since most of the electrons will be close to the bound energy value.

Since the probability of finding an electron in any given energy state was earlier expressed by,

$$Probability = \int \Psi_\lambda^* \Psi_\lambda dv \tag{4.71}$$

The total carrier concentration is therefore given by,

$$n = \sum_{\lambda=1}^{k} n_\lambda [|\Psi_\lambda^*||\Psi_\lambda|] \tag{4.72}$$

The carrier concentrations calculated from equation (4.72) are substituted in the Poisson's equation (4.33) and a new potential value is calculated. Equations (4.33), (4.51) and (4.72) are solved until a self-consistent solution is obtained.

Chapter 5

Results and Verifications

The verification of the semiconductor device simulator results was performed in two steps. First, the individual solvers were verified and then a complete self consistent simulation was performed and the results compared with a verifiable example. The device of choice for the verification of the self consistent solution was chosen to be a Silicon diode. A diode type device was chosen for the simplicity of its solution and for the well developed analytical equations whose solution can then be used for comparison with the simulated results.

5.1 Analytical Solution of the Silicon Diode

The Silicon diode used for the verification of the self consistent solution is shown in Figure 5.1. The material parameters used in the example are shown in Table 5.1. The equations and the results used in the analytical solution of the Silicon diode are in this chapter.

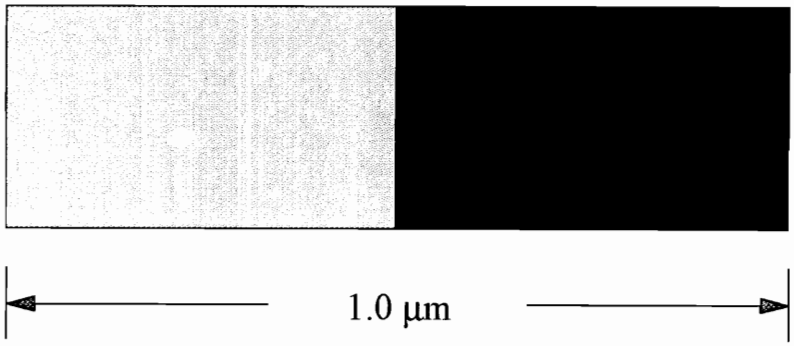

Figure 5.1, Dimensions of the Silicon Diode Used for Verification

TABLE 5.1

Material parameters used in simulation of Silicon Diode.

Relative permittivity, ε_r	*11.8*
Density of state effective masses	
Electron, m^*_e/m_0	m^*_{el}= *0.98,* m^*_{et}= *0.19*
Hole, m^*_h/m_0	m^*_{lh}= *0.16,* m^*_{hh}= *0.49*
Electron affinity (eV)	*4.05*
Band gap parameters	
$E_g(0)$ *(eV)*	*1.17*
α *(eV/K)*	4.73×10^{-4}
β *(K)*	*636*

All material parameters at 300 °K.

In order to calculate the built-in potential, V_{bi}, it is assumed that the majority carrier concentrations on the n and p sides are equal to the ionized impurity concentrations, N^{+}_{D} and N^{-}_{A}, respectively. The ionized impurity concentrations are computed by determining the quasi-fermi levels, E_{fn} and E_{fp}, using the charge neutrality condition under equilibrium. The density of states for the conduction and valence bands, N_C and N_V, are computed using the effective density of state masses, m^*_e and m^*_h, respectively. In Silicon, the conduction band varies differently in the longitudinal and transverse directions, thus giving two different electron effective masses, m_l^*, m_t^*. Therefore for electrons, the density of state effective mass, m_e^*, is given by [4.4],

$$m_e^* = \left(m_l^* \times (M_C \times m_t^*)^2 \right)^{1/3} \tag{5.1}$$

where,

M_C = Number of minimas in the conduction band (6 in Silicon).

Similarly for holes, due to the presence of light and heavy holes at the valence band edge, the density of state effective mass is given by,

$$m_h^* = \left[(m_{lh})^{3/2} + (m_{hh})^{3/2} \right]^{2/3} \tag{5.2}$$

Using parameters given in Table 5.1, we get;

$m_e^* = 1.084\, m_0\ kg.$

$m_h^* = 0.549\, m_0\ kg.$

Since, density of states for the conduction and valence bands are given by,

$$N_C = 2\left[\frac{m_e^* kT}{2\pi\hbar^2}\right]^{3/2} \tag{5.3}$$

$$N_V = 2\left[\frac{m_h^* kT}{2\pi\hbar^2}\right]^{3/2} \tag{5.4}$$

Therefore,

$N_C = 2.829 \times 10^{19}\ cm^{-3}$.

$N_V = 1.020 \times 10^{19}\ cm^{-3}$.

Using the temperature dependent band gap parameters, and equation (4.3), the band gap at 300°K is,

$E_g(300) = 1.1245\ eV$.

The intrinsic carrier concentration, n_i, is given by,

$$n_i = 2\left(\frac{kT}{2\pi\hbar^2}\right)^{1.5} (m_e^* m_h^*)^{0.75} exp\left(-\frac{E_g}{2kT/q}\right) \tag{5.5}$$

Using the charge neutrality conditions, the Fermi energy levels in the two regions of the diode are computed to be,

E_C-E_F = 0.9439 eV, *In the p-type region.*

E_C-E_F = 0.1469 eV, *In the n-type region.*

This gives the ionized impurity concentrations to be,

$N^-_A = 9.43 \times 10^{15}\ cm^{-3}$.

$N^+_D = 9.63 \times 10^{16}\ cm^{-3}$.

The built-in potential is computed using the above parameters and the computed value of the intrinsic carrier concentration, n_i. The built-in potential is given by,

$$V_{bi} = \frac{kT}{q} \ln\left(\frac{N^+_D N^-_A}{n_i^2}\right) \tag{5.6}$$

Substituting values in equation (5.6) gives,

$V_{bi} = 0.797\ V.$

Since there is no applied potential, therefore, the depletion region widths are given by,

$$x_n = \left[\frac{2\varepsilon_0\varepsilon_r V_{bi} N^-_A}{qN^+_D(N^-_A + N^+_D)}\right]^{1/2} \tag{5.7}$$

and

$$x_p = \left[\frac{2\varepsilon_0\varepsilon_r V_{bi} N^+_D}{qN^-_A(N^-_A + N^+_D)}\right]^{1/2} \tag{5.8}$$

Using the computed values for V_{bi}, N^{+}_{D}, and N^{-}_{A}, the depletion region widths are,

x_n = 0.031 μm.

x_p = 0.317 μm.

5.2 *Verification*

The Schrödinger wave equation solver and the Poisson's equation solver are verified separately. Once the two solvers have been verified, the final self consistent solution is obtained to verify the device simulator.

5.2.1 *Verification of the Schrödinger Wave Equation Solver*

The Schrödinger equation is used to compute the eigen values inside the diode. For device structures similar to a diode, where the energy bound is only on one side, the valid eigen energy values lie very close to the base energy. Thus for electrons in a diode, the p-side offers one energy barrier where as the contact side is unbounded, Figure 5.2. In such cases the number of valid eigen energy values is as large as the number of discritized points on the n-side. Thus, for devices with large number of discritized points, it becomes difficult to verify the eigen values and eigen vectors, using a diode example. Therefore, in order to perform initial verification of the Schrödinger equation, an example with bounded eigen energy values was selected, e.g. eigen values and eigen vectors in a quantum well.

The example selected to verify the Schrödinger wave equation solver is outlined below [2.25].

To verify the Schrödinger wave equation solution, a single quantum well, resulting from the heterointerface of GaAs/$Al_{0.3}Ga_{0.7}As$, is chosen. The dimensions of the quantum well are shown in Figure 5.3.

The eigen energy values of this finite barrier potential well are [2.25],

$E_1 = 64.24722\ meV.$

$E_2 = 220.7776\ meV.$

Figure 5.4 shows the computed eigen values and eigen vectors for the quantum well. The error in the computed results when compared to the exact solution is less than 0.2%.

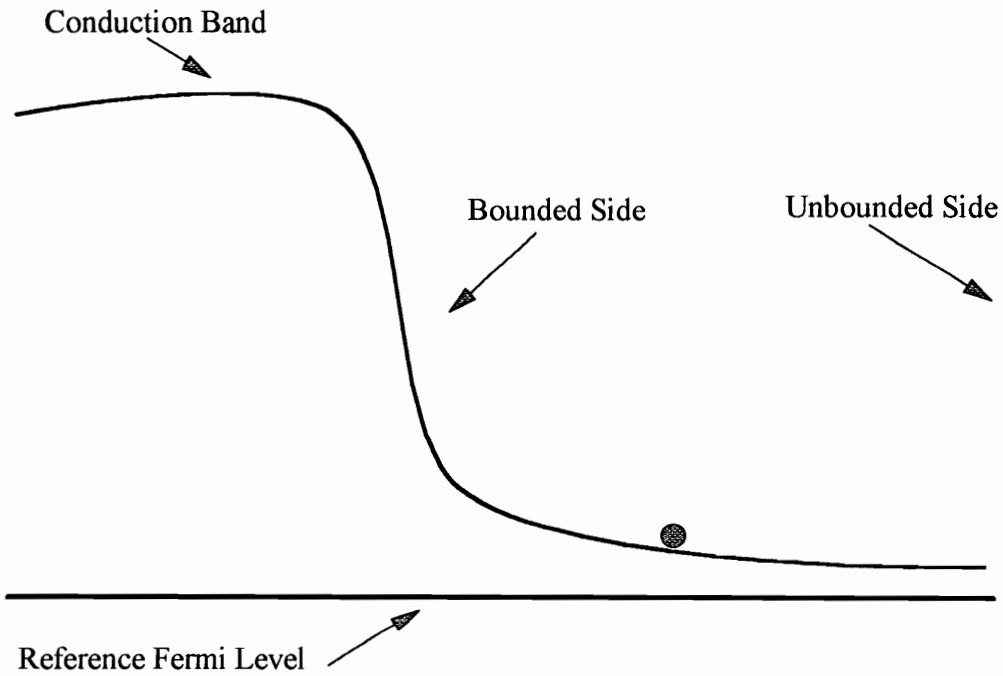

Figure 5.2, Energy Bounds for an Electron in the Conduction Band

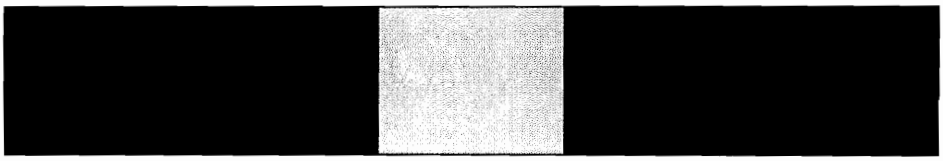

$Al_{0.3}Ga_{0.7}As$ GaAs $Al_{0.3}Ga_{0.7}As$

$\Delta E_C = 0.23$ eV

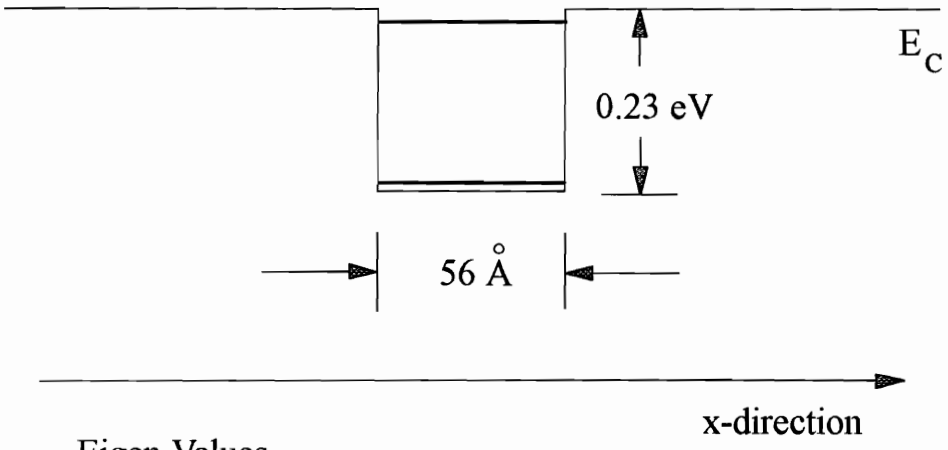

Eigen Values

$E_1 = 220.7776$ eV

$E_2 = 64.24722$ eV

Figure 5.3, GaAs/$Al_{0.3}Ga_{0.7}As$ Quantum Well Structure

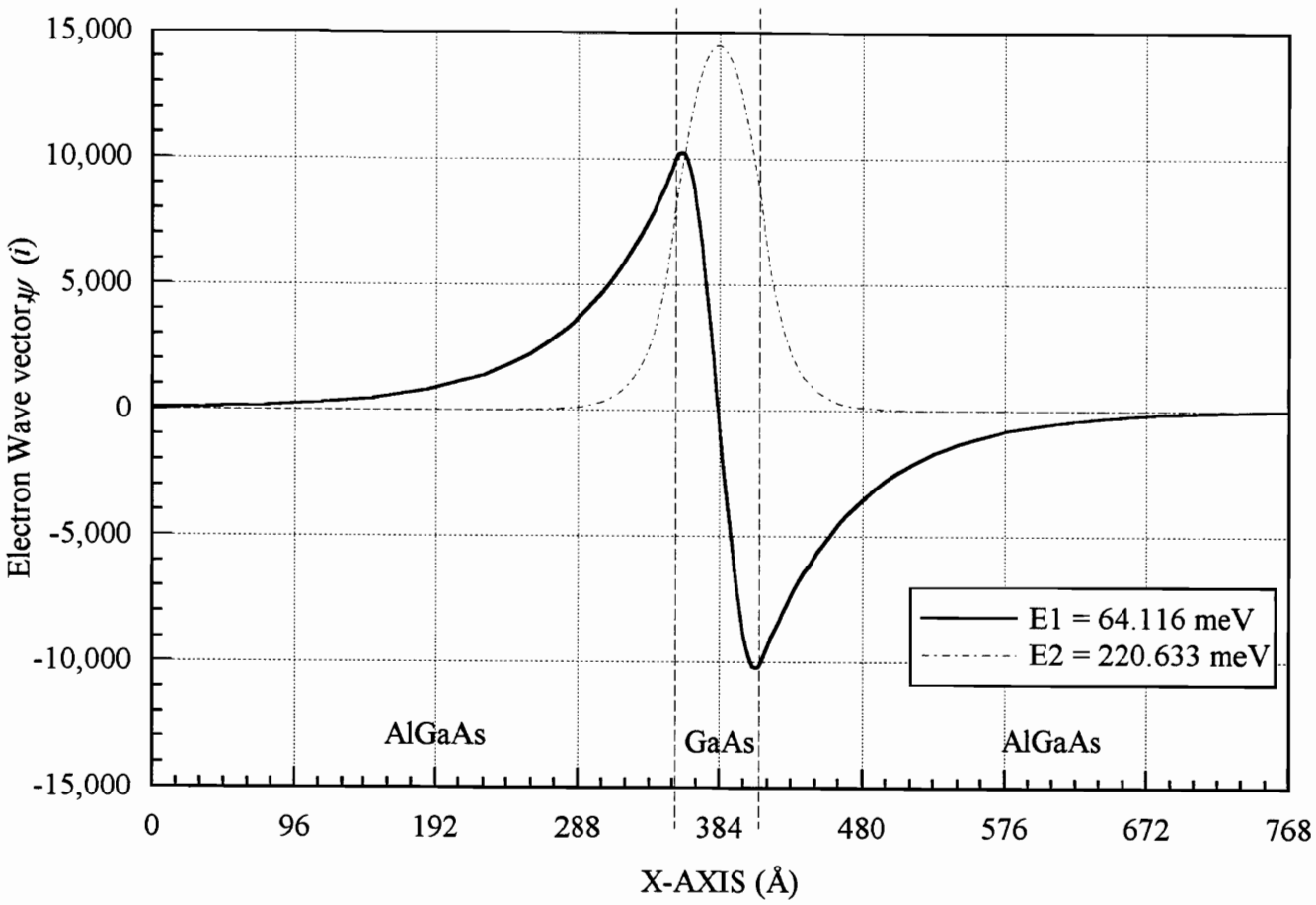

Figure 5.4, Eigen Values and Eigen Vectors Computed Using the Schrodinger Equation Solver

5.2.2 Verification of the Poisson's Equation Solver

The Poisson's equation solver's verification can be performed in two ways. For an unbiased diode the potential distribution resulting from the solution of the Poisson's equation must be equal to the built in potential. One method of determining the built-in potential is to find the difference in the Fermi levels on the n and p sides of the diode. This method only confirms the magnitude of the built-in potential and not the built-in potential profile. The second method is used to verify the built-in potential profile as well as the magnitude. In the second method, the electric field inside the diode is determined from the analytical equations. This electric field is then integrated over the length of the diode to obtain the potential profile inside the diode. The simulated potential, on the other hand, is obtained by generating a depletion region inside the diode and computing the potential profile inside the diode using the Poisson's equation solver. The reason for providing the depletion region information to the simulator is that, in a self consistent simulation the depletion region is formed due to the carrier solution obtained from the Schrödinger equation solver. When only using the Poisson's equation solver, this feedback is missing and one has to provide this information.

The depletion region estimate is based on the values computed from the analytical solution. Inside the depletion region the mobile carrier concentration is forced to zero. The fixed charge density is taken to be the ionized impurity concentrations. The potential

distribution inside the diode, obtained from the solution of the Poisson's equation is shown in Figure 5.5. The simulated potential was pinned down to *0.0* volts at the center. Pinning down the potential is necessary so as to obtain faster convergence. Pinning down of the potential does not effect the computed results, since the Poisson's equation is only used to provide the relative magnitude of the conduction and valence band energies. Therefore, only the shape of the potential profile, which is the shape of the conduction and valence bands along with appropriate band offsets at the heterointerface, is needed. Figure 5.6, shows the relative error in the solution of the Poisson's equation. The error is comparatively larger on the *p*-side of the diode than on the *n*-side, due to the fact that the *p*-side has doping concentration an order of magnitude less than the *n*-side. This causes the depletion region to be mostly on the *p*-side and consequently the potential variation inside the diode to be mostly confined to the *p*-side. A comparison of the results obtained from the simulation of the Poisson's equation and the analytical solution is shown in Figure 5.7.

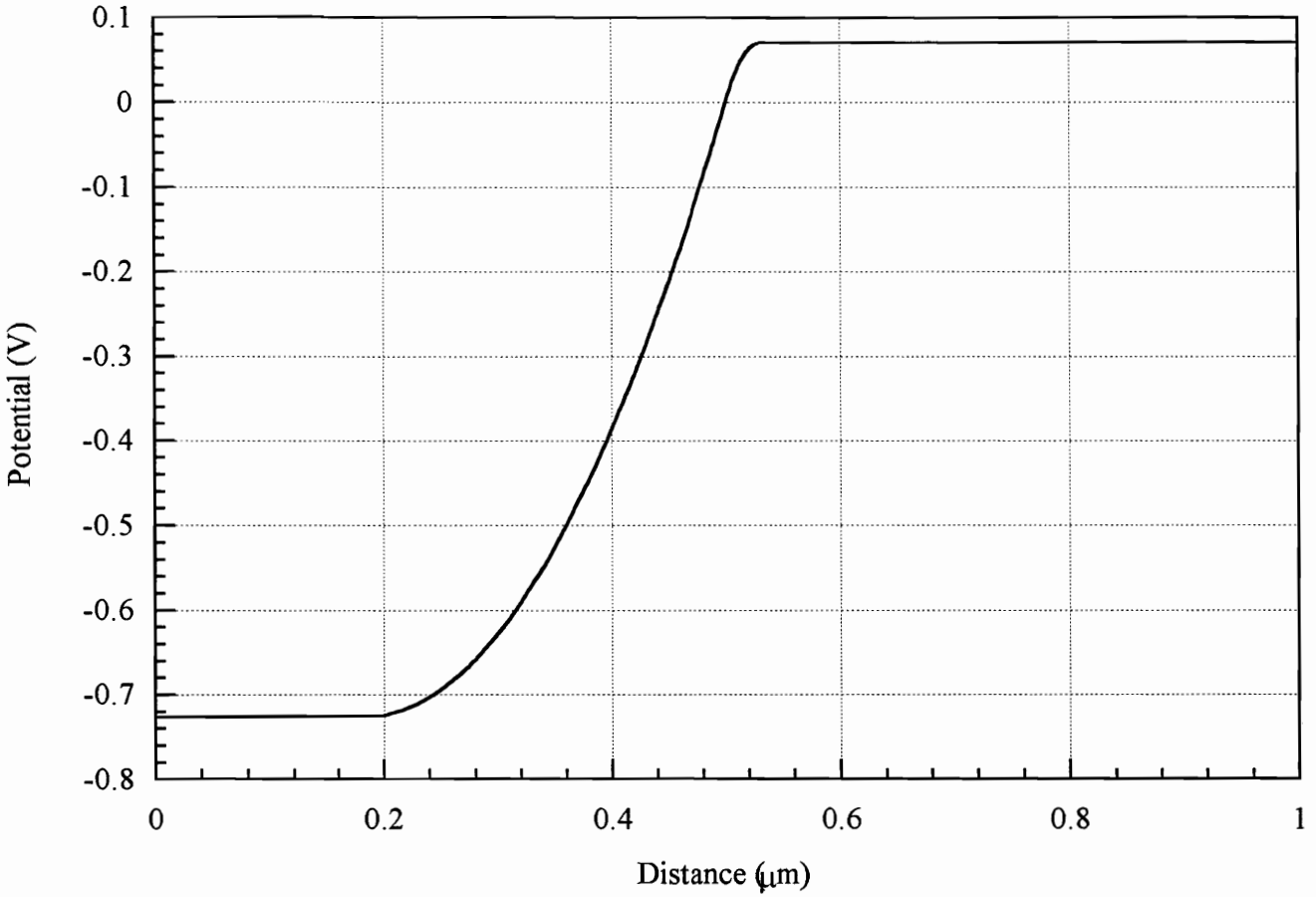

Figure 5.5, Potential Distribution Obtained Using the Poisson Equation Solver

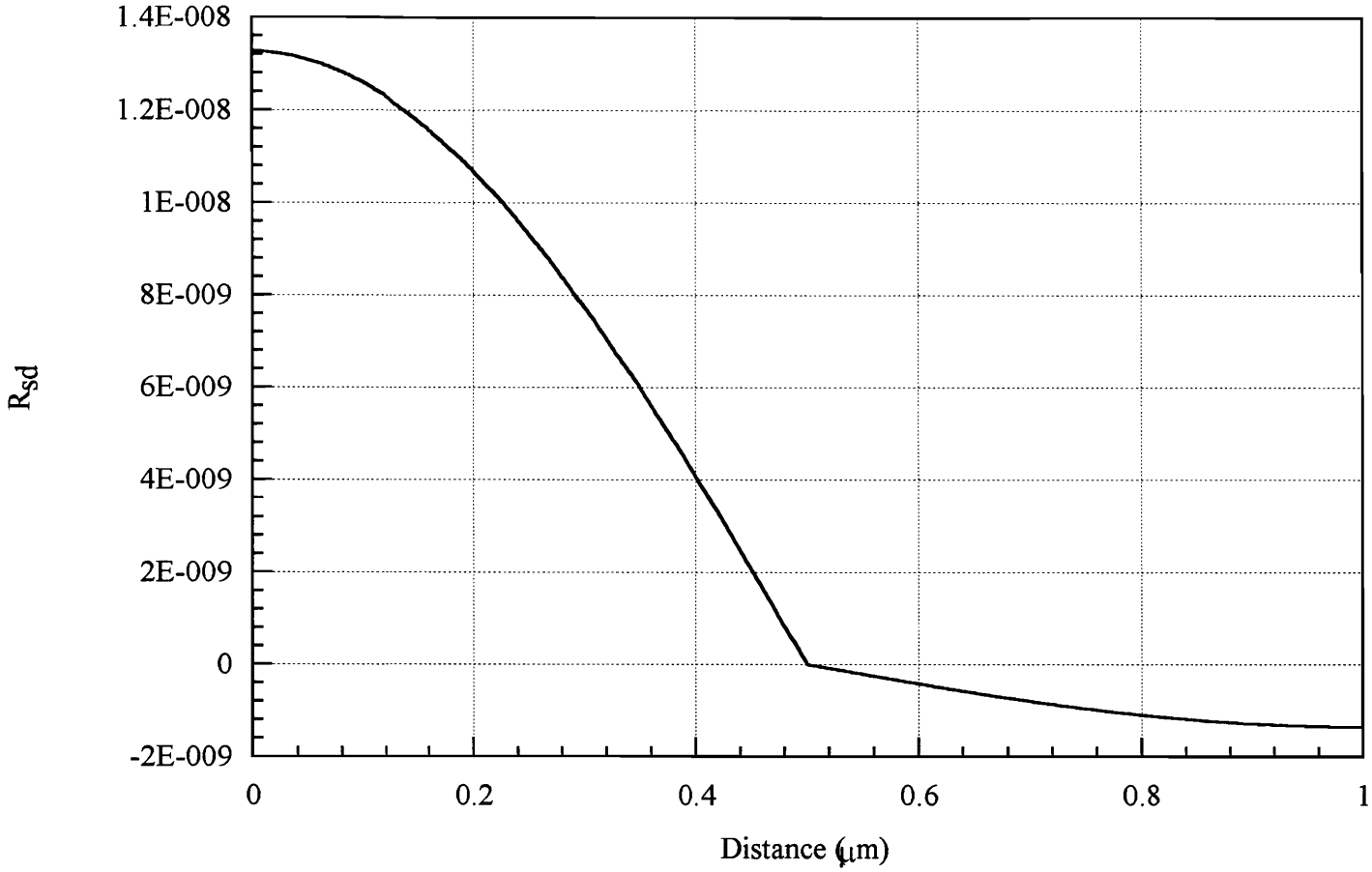

Figure 5.6, Residual Error in the Solution Obtained from Poisson's Equation

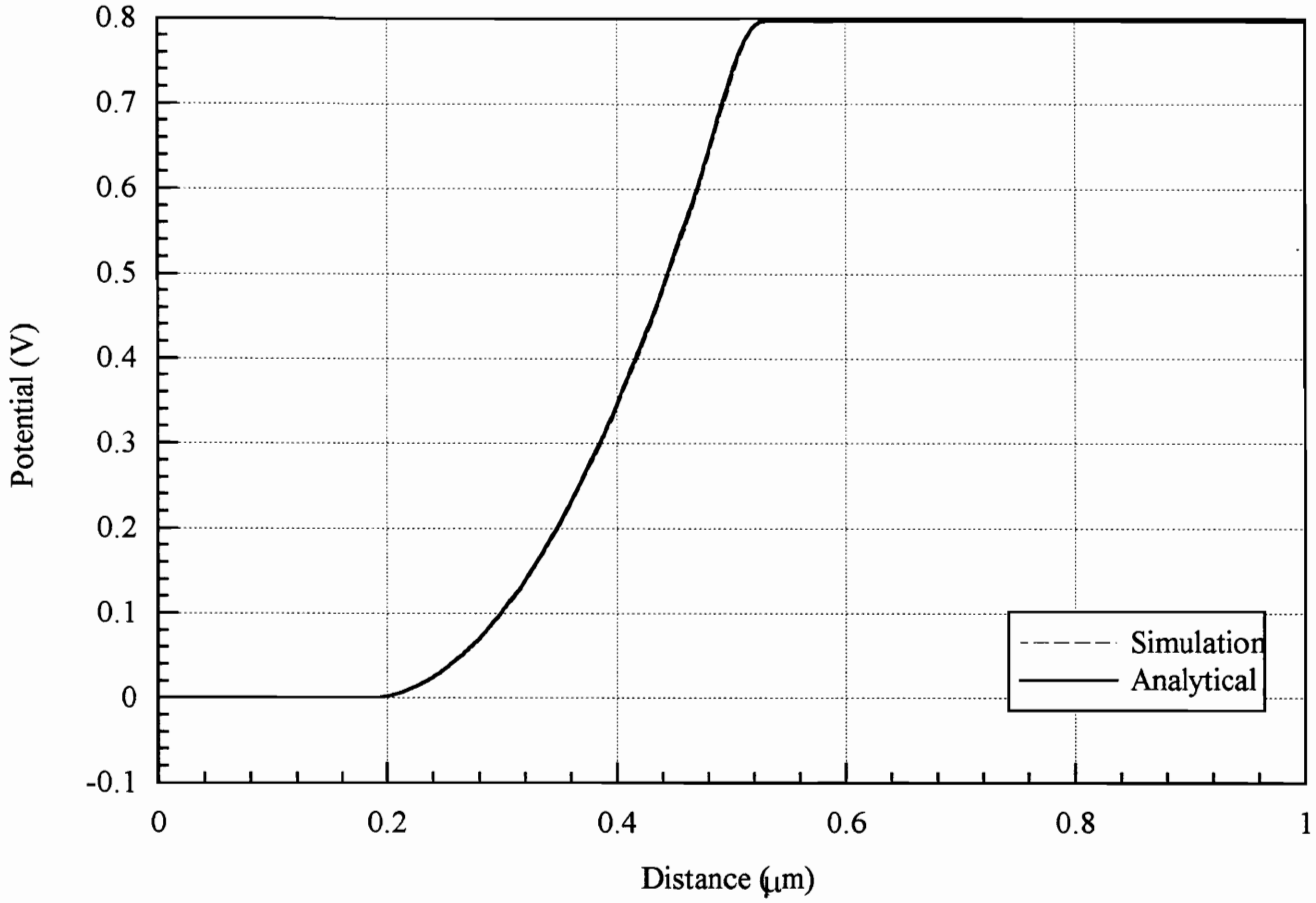

Figure 5.7, Comparison of Simulated and Analytically Obtained Potential Distributions

5.3 Verification of the self consistent solution

Self consistent solution is obtained by first computing the Fermi levels in the two regions of the diode. Based on these Fermi levels the ionized donor and acceptor impurities are computed for the particular operating temperature. The initial electron and hole concentrations are put equal to the ionized donor and acceptor impurity levels, respectively. These concentrations are then substituted in the Poisson's solver along with the initial estimate for the potential distribution inside the diode. The Poisson's equation is solved and the updated potential distribution is used to obtain the valence and conduction band profiles. These band profiles are then used in the Schrödinger equation solver to solve for the electron and hole wave vectors and corresponding eigen energy values. The electron and hole wave vectors and the corresponding eigen energy values are then used to compute the updated carrier concentrations. The updated carrier concentrations are then re-substituted in the Poisson's equation solver to update the potential profile once again. This process is repeated in a self consistent manner, until the error criteria has been met. Based on the final potential profile inside the diode, the conduction and valence band profiles are shown in Figure 5.8. The final electron and hole concentration profiles are shown in Figure 5.9. For the charge neutrality condition to hold, these concentrations must equal the ionized impurity concentrations. The errors in the upper bound of the electron and hole concentrations when compared to with the ionized impurity concentrations are less than 3.3% and 5.9%, respectively.

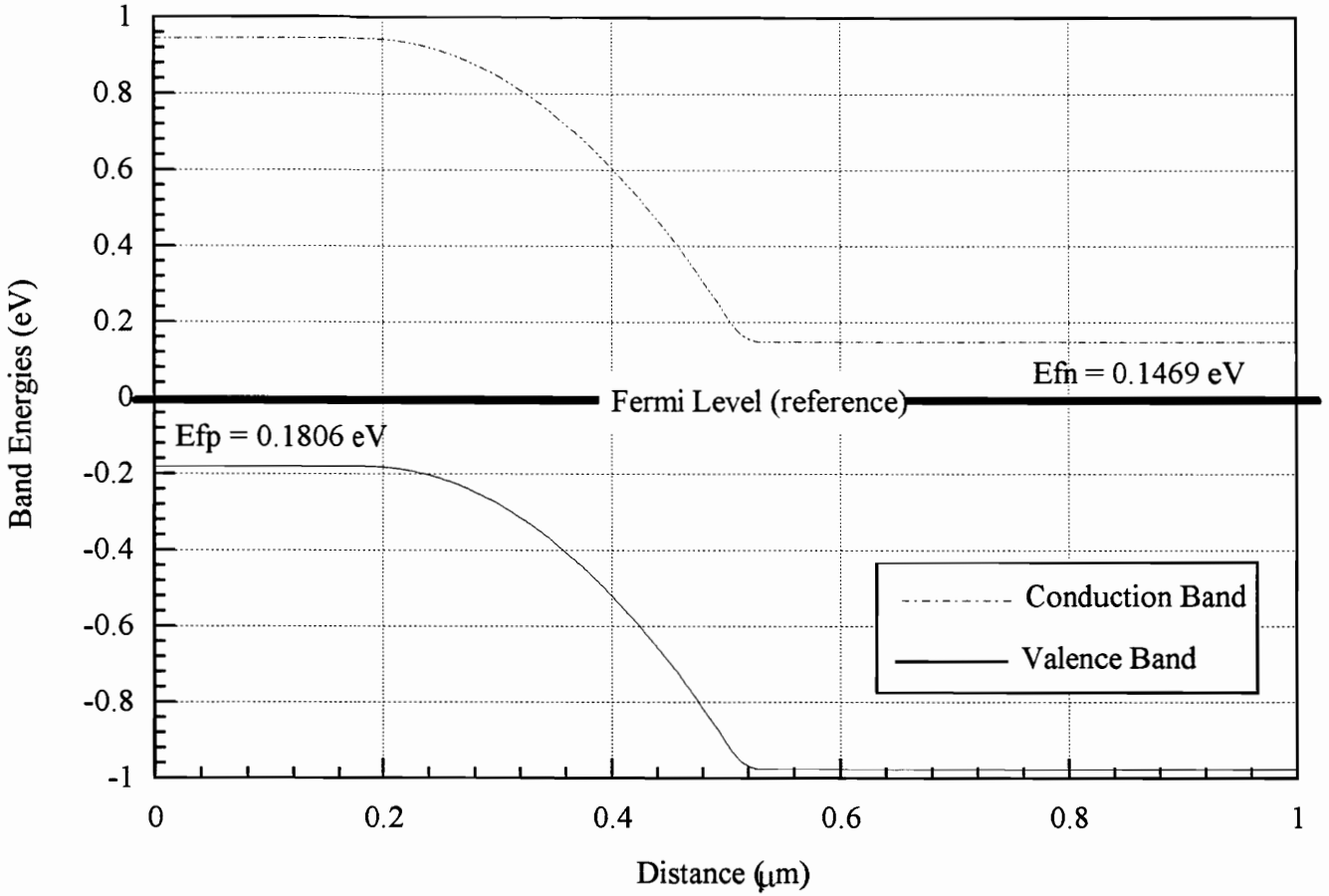

Figure 5.8, Self-consistent Energy Band Profiles Inside the Diode

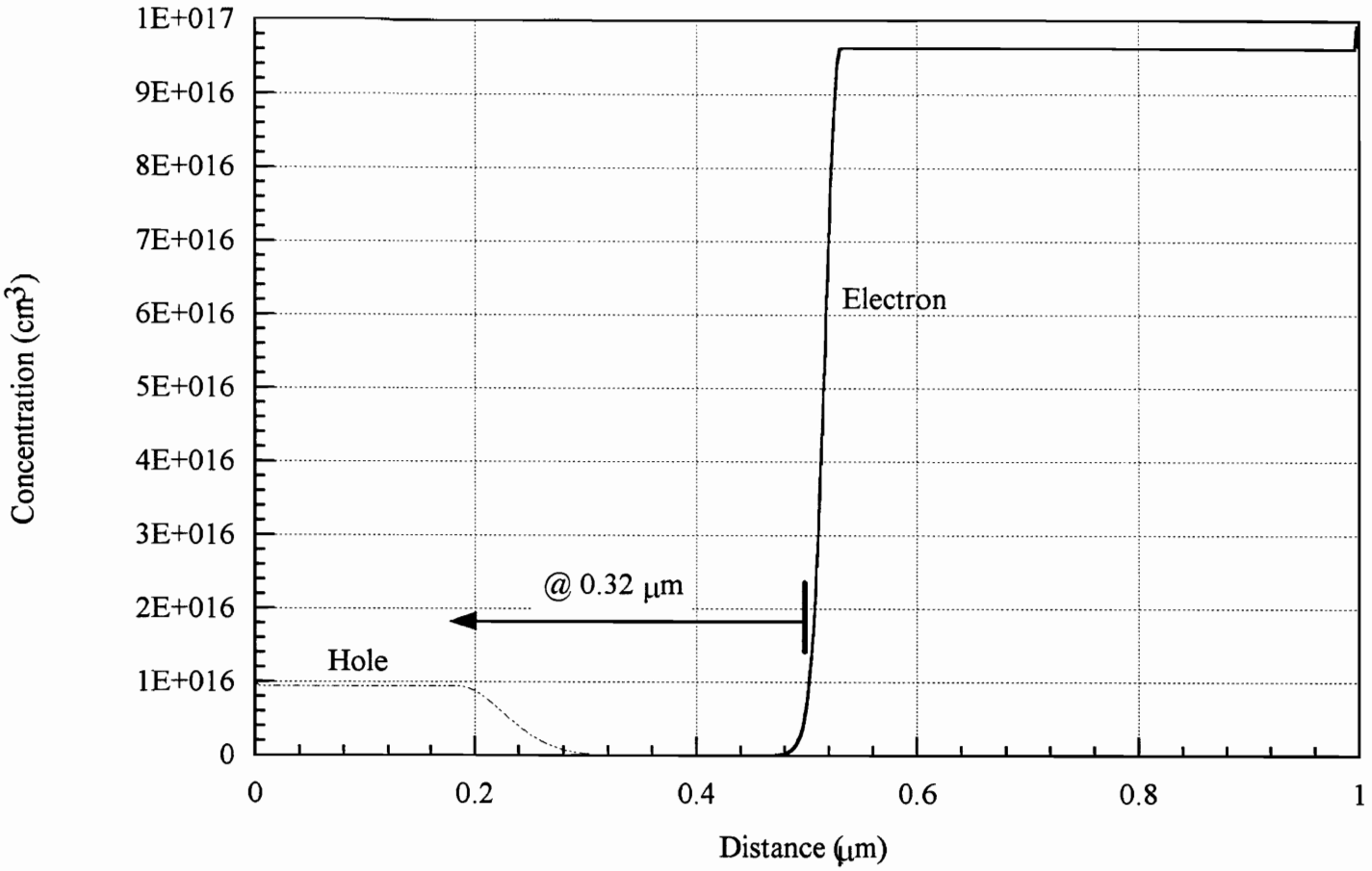

Figure 5.9, Self-consistent Electron and Hole Concentrations

Chapter 6

Summary and Conclusion

The quantum mechanical semiconductor device simulator described in this work is based on the self-consistent solution of Poisson's and Schrödinger equations. Using an initial estimate for the carrier concentrations and the potential distribution inside the semiconductor device, the Poisson's equation is solved to obtain the updated potential distribution. The updated potential distribution from the Poisson's equation is then used in the Schrödinger equation to get valid eigen values and eigen vectors for both the electrons and holes. These eigen values and eigen vectors are then used to calculate the carrier concentrations. The updated carrier concentrations are substituted back into the Poisson's equation to further update the potential distribution. The process is repeated until a self-consistent solution is obtained.

In this work, multiple carrier simulation using quantum mechanical principles has been performed. The simulation uses a more appropriate 3-D density of state function for calculating the carrier concentrations. A dual carrier quantum mechanical semiconductor device simulator has the advantage of accurately simulating small geometry devices, as well as simulation of quantum effects such as quantum confinement. The work can be further extended to apply to modeling of optical effects, and computation of the carrier currents using the electric field dependent mobility information.

The decision whether to use an equivalent circuit model or a device simulator depends upon the designer and the required accuracy of prediction. To save computational time, one should use as simple a model as the accuracy will allow. At this time, however, the trend is towards developing quantum mechanical models which are more accurate and, with faster computers available, the computational time for these simulators has been considerably reduced.

References

[1.1] H. B. Bakoglu, *Circuits, Interconnections, and Packaging for VLSI*, Addison-Wesely Publishing Company, 1990.

[1.2] Tony Hey and Patrick Walters, *The Quantum Universe*, Cambridge University Press, 1987.

[2.1] I. Getreu, *Modeling The Bipolar Transistor,* Tektronix Inc. , 1976.

[2.2] C. M. Snowden, *Semiconductor Device Modeling,* Peter Peregrinus Ltd, 1988.

[2.3] J. J. Ebers and J. L. Moll, "Large Signal Behavior of Junction Transistors," *Proc. IRE*, vol. 42, pp. 1761-1772, Dec 1954.

[2.4] H. K. Gummel and H. C. Poon, "An Integral Charge Control Model of Bipolar Transistors," *Bell Syst. Tech. J.,* vol. 49, pp. 827-852, May-June 1970.

[2.5] L. W. Nagel and D. O. Pederson, "Simulation Program with Integrated Circuit Emphasis (SPICE)," 16th Midwest Symposium on Circuit Theory, Waterloo, Ontario, April 12, 1973.

[2.6] T. E. Idleman, F. S. Jenkins, W. J. McCalla and D. O. Pederson, "SLIC - A Simulator for Linear Integrated Circuits," *IEEE J. Solid State Circuits,* vol. SC-6, pp. 188-203, 1971.

[2.7] S. P. Fan and D. O. Pederson, "SINC, A nonlinear DC and Transient analysis program".

[2.8] H. J. Deman and R. Mertens, "SITCAP - A Simulator of Bipolar Transistors for Computer-aided circuit analysis Programs," *ISSCC Digest of Technical Papers,* pp. 104-105, 1973.

[2.9] C. M. Snowden, *Introduction to Semiconductor Device Modelling,* World Scientific, 1986.

[2.10] W. L. Engl, *Process and Device Modeling,* North-Holland, 1986.

[2.11] Mark S. Lundstrom and Robert John Schuelke, "Numerical analysis of Heterostructure Semiconductor Devices," *IEEE Trans. Electron Devices,* vol. ED-30, No. 9, pp 1151-1159, 1983.

[2.12] Akira Yoshii, Hitoshi Kitazawa, Masaaki Tomzawa, Shoji Horiguchi and Tsuneta Sudo, "A Three Dimensional Analysis of Semiconductor Devices," *IEEE Trans. Electron Devices,* vol. ED-29, No. 2, pp 184-189, 1982.

[2.13] D. L. Scharfetter and H. K. Gummel, "Large-signal analysis of a silicon read diode oscillator," *IEEE Trans. Electron Devices*, vol. ED-16, No. 1, pp. 64-77, 1969.

[2.14] Akira Yoshii, Hitoshi Kitazawa, Masaaki Tomizawa, Shoji Horiguchi, and Tsuneta Sudo, "A Three-Dimensional Analysis of Semiconductor Devices," *IEEE Trans. Electron Devices,* vol. ED-29, No. 2, pp 184-189, 1982.

[2.15] Ryota Kasai, Kiyoyuki Yokoyama, Akira Yoshii and Tsuneta Sudo, "Threshold-Voltage Analysis of Short- and Narrow-Channel MOSFETs by Three-Dimensional Computer Simulation," *IEEE Trans. Electron Devices,* vol. ED-21, No. 5, pp 870-876, 1982.

[2.16] M A R Al-Mudares, and B K Ridley, "Monte Carlo simulation of scattering-induced negative differential resistance in AlGaAs/GaAs quantum wells," *J. Phys. C: Solid State Phys.* vol. 19, pp. 3179-3192, 1986.

[2.17] Sorin Voinigescu, "Quantum modelling of charge distribution in single and multiple heterojunction modfets," *Int. J. Electronics*, vol. 66, No. 2, pp. 227-245, 1989.

[2.18] I-H. Tan, G. L. Snider, L. D. Chang, and E. L. Hu, "A self-consistent solution of Schrodinger-Poisson equations using nonuniform mesh," *J. Appl. Phys.* vol. 68, No. 8, pp. 4071-4076, 1990.

[2.19] G. L. Snider, I-H. Tan, and E. L. Hu, "Electron states in mesa-etched one-dimensional quantum well wires," *J. Appl. Phys.* vol. 68, No. 6, pp. 2849-2853, 1990.

[2.20] Kiyoyuki Yokoyama, Masaaki Tomizawa, Akira Yoshii and Tsuneta Sudo, "Semiconductor Device Simulation at NTT," *IEEE Trans. Computer-Aided Design,* vol. CAD-4, No. 4, pp. 452-460, 1985.

[2.21] M. R. Pinto, C. S. Rafferty and R. W. Dutton, "PISCES-II: Poisson and continuity equation solver," Stanford Electronics Lab. Tech. Rep., Sept. 1984.

[2.22] PISCES-2B and DAVINCI are softwares developed by TMA Inc., Palo Alto CA 94301.

[2.23] S. Selberherr, A. Schutz and H. W. Potzl, "MINIMOS-A two dimensional MOS transistor analyzer," *IEEE Trans. Electron Devices,* vol. ED-27, pp. 1540, 1980.

[2.24] A. F. Franz and G. F. Franz, "BAMBI user's guide," Technische Univ. Wien, Vienna, Austria,1985.

[2.25] Jue-Hsien Chern, John T. Maeda, Lawrence A. Arledge, Jr. and Ping Yang, "SIERRA: A 3-D Device Simulator for Reliability Modeling," *IEEE Trans. Computer-Aided Design,* vol. CAD-8, No. 5, pp. 516-527, 1989.

[2.26] Toru Toyabe, Hiroo Masuda, Yukio Aoki, Hiroko Shukuri and Takaaki Hagiwara, "Three-Dimensional Device Simulator CADDETH with Highly Convergent Matrix Solution Algorithms," *IEEE Trans. Electron Devices,* vol. ED-32, No. 10, pp 2038-2044, 1985.

[2.27] Clifford M. Krowne, "Semiconductor Heterostructure Nonlinear Poisson Equation," *J. Appl. Phys.* vol. 65, No. 4, pp. 1602-1614, 1989.

[2.28] G. W. Brown, and B. W. Lindsay, "The Numerical Solution of Poisson's Equation for Two-Dimensional Semiconductor Devices," *Solid-State Electronics*, vol. 19, pp. 991-992, 1976.

[2.29] John J. Barnes, and Ronald J. Lomax, "Finite-Element Methods in Semiconductor Device Simulation," *IEEE Trans. Electron Devices,* vol. ED-24, No. 8, pp. 1082-1089, 1977.

[2.30] Tohru Adachi, Akira Yoshii, and Tsuneta Sudo, "Two-Dimensional Analysis using Finite-Element Method," *IEEE Trans. Electron Devices,* vol. ED-26, No. 7, pp. 1026-1031, 1979.

[2.31] Gen-Lin Tan, Xiao-Li Yuan, Qi-Ming Zhang, Walter H. Ku, and An-Jui Shey, "Two-Dimensional Semiconductor Device Analysis Based on New Finite-Element Discritization Employing the S-G Scheme," *IEEE Trans. Computer-Aided Design,* vol. CAD-8, No. 5, pp. 468-478, 1989.

[2.32] E. M. Buturla, P. E. Cottrell, B. M. Grossman, K. A. Salsburg, "Finite-Element Analysis of Semiconductor Devices: The FIELDAY Program," *IBM J. Res. Develop.*, 25, 218-231 (1981).

[2.33] G. T. Symm, "Boundary Element Applications in Electrostatics," *Heat Transfer, Fluid Flow & Electrical Applications*, pp.383-397.

[2.34] G. S. Gipson, "Progress in The Analysis of Poisson-Type Problems by Boundary Elements," *Heat Transfer, Fluid Flow & Electrical Applications*, pp.101-113.

[2.35] G. de Mey, and F. Cuypers, "The Boundary Element Method for Semiconductor Device Analysis," *Heat Transfer, Fluid Flow & Electrical Applications*, pp.399-415.

[2.36] Randolf E. Banks, Donald J. Rose and Wolfgang Fichtner, "Numerical Methods for Semiconductor Device Simulation," *IEEE Trans. Electron Devices,* vol. ED-30, No. 9, pp. 1031-1041, 1983.

[2.37] Andrea F. Franz, Gerhard A. Franz, Siegfried Selberherr, Christian Ringhofer and Peter Markowich, "Finite Boxes - A Generalization of the Finite-Difference Method Suitable for Semiconductor Device Simulation," *IEEE Trans. Electron Devices,* vol. ED-30, No. 9, pp. 1070-1082, 1983.

[3.1] W. Kohn, and J. M. Luttinger, "Quantum Theory of Electrical Transport Phenomena," Physical Review, vol. 103, No. 3, pp. 590-611, 1957.

[3.2] Leonard I. Schiff, *Quantum Mechanics 3/e,* McGraw-Hill, 1987.

[3.3] Michael Shur, *Physics of Semiconductor Devices,* Prentice Hall, 1990.

[3.4] D. K. Ferry, and J. R. Barker, "On The Physics and Modeling of Small Semiconductor Devices-III: Transient response in the finite collision-duration regime," *Solid-State Electronics*, vol. 23, pp. 545-549, 1980

[4.1] S. M. Sze, *Physics of Semiconductor Devices 2/e*, John Wiley & Sons, 1981.

[4.2] Kiyoyuki Yokoyama, Masaaki Tomizawa, Hiroshi Kanbe, and Tsuneta Sudo, "A Numerical Analysis of a Heterostructure InP/InGaAs Photodiode," *IEEE Trans. Electron Devices,* vol. ED-30, No. 10, pp. 1283-1288, 1983.

[4.3] Ward Cheney, and David Kincaid, *Numerical Mathematics and Computing 2/e*, Brooks / Cole Publishing Company, 1985.

[4.4] Jasprit Singh, *Semiconductor Devices, An Introduction*, McGraw-Hill, Inc., 1994.

Vita

The author was born in Peshawar Pakistan on February 12, 1962. He received his Bachelor of Science in Electrical Engineering form N.W.F.P. University of Engineering and Technology, Peshawar, Pakistan in 1984.

In 1985 he joined The Water and Development Authority of Pakistan as Junior Engineer, responsible for the operation of a Hydroelectric Power Station.

In 1988 he obtained his Master of Science in Electrical Engineering from The University of Michigan, Ann Arbor. He came to Virginia Polytechnic Institute and State University in 1990 to pursue a Doctorate of Philosophy in Electrical Engineering. In 1993 he became a Research Associate with the Microelectronics and Microwave Material Characterization groups in the Bradley Department of Electrical Engineering. His main areas of interests are semiconductor device simulation as well as design and fabrication of hybrid circuits including packaging for electronic circuits and devices.